CHALMERS
UNIVERSITY OF TECHNOLOGY

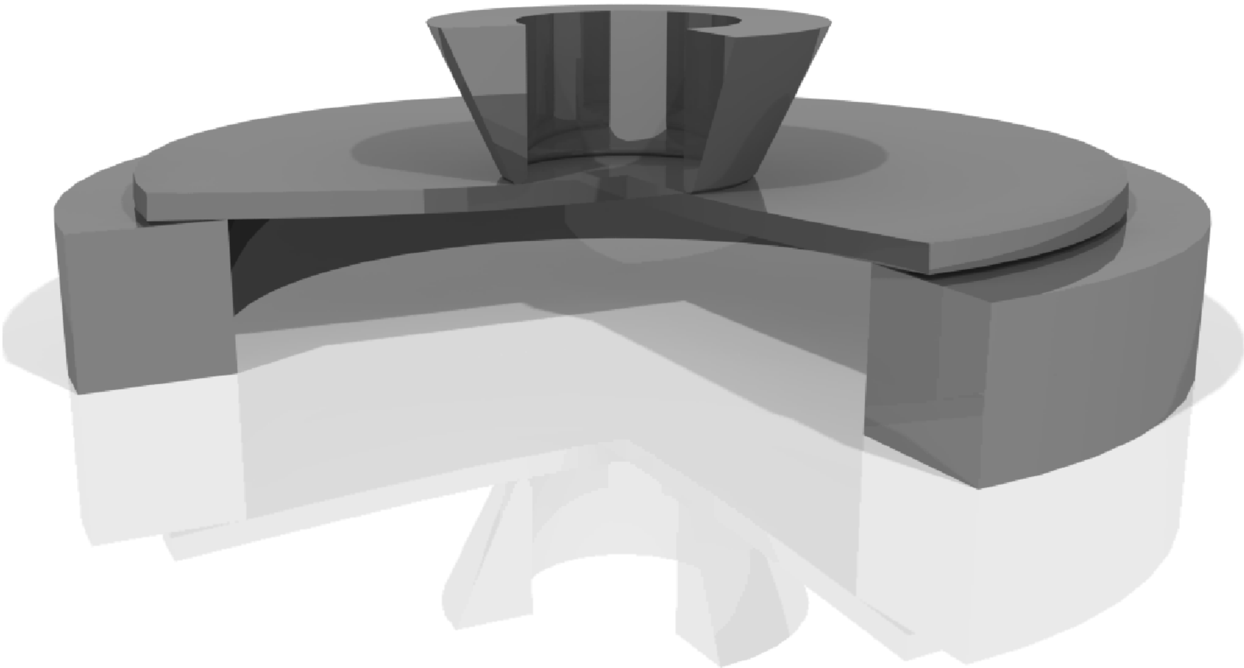

Design of Experiments for Validation of Multiaxial High Cycle Fatigue Criteria

Master's Thesis in Applied Mechanics

NIKLAS OLOFSSON

Department of Applied Mechanics
CHALMERS UNIVERSITY OF TECHNOLOGY
Gothenburg, Sweden 2017

Master's thesis 2017:04

Design of Experiments for Validation of Multiaxial High Cycle Fatigue Criteria

NIKLAS OLOFSSON

CHALMERS
UNIVERSITY OF TECHNOLOGY

Department of Applied Mechanics
Division of Dynamics
Chalmers University of Technology
Gothenburg, Sweden 2017

Design of Experiments for Validation of Multiaxial High Cycle Fatigue Criteria
NIKLAS OLOFSSON

Supervisor: Rebecka Brommesson & Gunnar Högström, GKN Aerospace Sweden
Examiner: Anders Ekberg, Chalmers University of Technology

Master's Thesis 2017:04
Department of Applied Mechanics
Division of Dynamics
Chalmers University of Technology
SE-412 96 Gothenburg
Telephone +46 31 772 1000

Cover: Proposed biaxial fatigue testing technique using a disc shaped specimen, supported at its edges and transversely loaded in the centre.

Typeset in LaTeX
Gothenburg, Sweden 2017

Design of Experiments for Validation of Multiaxial Fatigue Criteria
NIKLAS OLOFSSON
Department of Applied Mechanics
Chalmers University of Technology

Abstract

GKN Aerospace is a world leading supplier of aerospace engine components, continuously improving their design methods. One important area is the evaluation of high cycle fatigue (HCF) at multiaxial stress states. A critical plane criterion has been suggested to replace the currently used invariant criterion in order to improve accuracy. However, experiments are required to support and verify the choice of criterion.

Through a numerical comparison of criteria, states of stress where predictions differ are identified. Among them, biaxial stress states with high mid stresses are of special interest since such are often present in rotating engine components. Therefore, a testing method able to generate this state of stress is desirable.

A literature review shows that the two most commonly used biaxial testing methods are cruciform specimens loaded in two directions, and tubular specimens with internal pressure. However, both methods require complex, expensive and rare laboratory equipment. Hence, alternative methods are sought. Several concepts are developed and their feasibility are evaluated through numerical simulations. Recommendations regarding specimen geometry, test setup and failure detection are given. Finally, advantages and concerns for the concepts are summarised.

The Disc bending-concept is considered to be most promising. It constitutes a disc-shaped specimen, simply supported at its edges and transversely loaded in the centre region. This set up creates a biaxial bending stress state, with a close to uniform stress distribution. The concept may be thought of as a biaxial version of the uniaxial four point bending technique.

Keywords: Multiaxial Fatigue, Biaxial Fatigue Testing, High Cycle Fatigue, Test Specimen, Testing Method, Disc Bending

Acknowledgements

This master's thesis was written as the final part of the master's degree programme in Applied Mechanics at Chalmers University of Technology. It has been carried out at GKN Aerospace Sweden in Trollhättan during the autumn of 2016. My supervisors Rebecka Brommesson and Gunnar Högström have been supporting me continuously thorough the project. I would like to thank them for their invaluable help. My examiner, professor Anders Ekberg at the Department of Applied Mechanics, has been a great source of inspiration and earned my gratitude. Through his critical mind and external view on the project, he has contributed with important input. I would also like to thank the employees at the R&T-department, especially Jens Juul, Thomas Hansson and Anders Wretland for their helpful manner and patience with my questions.

Niklas Olofsson
Trollhättan, January 2017

Nomenclature

Abbreviations

FE	Finite Element
GAS	GKN Aerospace Sweden
HCF	High Cycle Fatigue
LCF	Low Cycle Fatigue
VHCF	Very High Cycle Fatigue

Symbols

N_f	Number of cycles to failure
R	Ratio between minimum and maximum stress for cyclic loading
SF	Scaling Factor, measure of fatigue risk for a certain stress state
UF	Utilization Factor, measure of fatigue risk for a certain stress state
TF	Triaxiality Factor, measure of multiaxiality for a stress state
$\sigma_1, \sigma_2, \sigma_3$	Principal stresses
σ_a	Amplitude stress (scalar)
$\bar{\sigma}_\mathrm{a}$	Amplitude stress tensor
σ_eq	Equivalent stress for a multiaxial stress state
σ_h	Hydrostatic pressure
σ_m	Mid stress (scalar)
$\bar{\sigma}_\mathrm{m}$	Mid stress tensor
σ_vM	von Mises effective stress
τ_Tr	Tresca effective stress

Contents

1
Introduction

A typical passenger aircraft will fly a distance equivalent to 2500 circumnavigations of the earth during its lifetime. If the aircraft weight can be reduced by 1 %, this will yield a lifetime saving of one million liters of jet fuel [1]. This will lower climate impact and also make the aircraft more competitive from an economic point of view. The structural design of the aircraft components is of utter importance, to save this weight while still maintaining safety and reliability. To achieve this, the structural design methods must be steadily improved.

1.1 Background

GKN Aerospace Sweden (GAS) is a world leading supplier of engine components for aircrafts, continuously investing resources in improving their design methods. Within the structural design of engine components, one of the major concerns is High Cycle Fatigue (HCF).

Many components in the aircraft engine are subjected to interacting loads. For example, the rotor blades in the engine are subjected to both inertial loads from rotation, and cyclic loads induced by air flow and vibration. This will often lead to a multiaxial state of stress in the component, which makes the fatigue evaluation more complicated. The basic methods of predicting HCF under uniaxial loading are in a large extent commonly accepted, but how to account for multiaxial effects is still an issue. Researchers have proposed numerous methods, but no best practice has been agreed on.

Investigations indicate that the stress invariant based Sines criterion used today at GAS may be overly conservative for some stress states, especially high biaxial mid stresses. Alternative criteria should therefore be considered. Research within the area suggests that critical plane criteria may be more accurate for complex multiaxial stress states. Among these criteria, the Findley criterion has shown good prospects and will be further investigated [2]. However, experiments are needed to support the choice of suitable criterion.

1.2 Aim

The main objective of this thesis is to propose a testing method that will be able to support in the choice of criterion. These tests will also serve as a validation of the criterion. A suitable testing method should meet the following requirements:

- Have a similar stress state as the rotating engine components. Typical for these components are high biaxial mid stresses.
- Clarify strengths and weaknesses of the compared criteria. Regions in the stress space where the predictions from the compared fatigue criteria differ are of special interest.
- Be feasible from an economic point of view. The limiting factors are further described in the next section.

1.3 Scope

This thesis will guide in the choice of testing method for multiaxial HCF, but performing the tests are not within the scope of the project. A comparison of established methods as well as alternative concepts will be given, outlining advantages and concerns. Recommendations regarding specimen geometry, test setup and failure detection for each concept will be presented.

Numerous criteria have been proposed in scientific papers, see e.g the overview in [3]. However, it is not uncommon that proposed criteria are computationally demanding and may require large amounts of test data for calibration. This project will only focus on some selected fatigue criteria that were suggested in a literature review performed at GAS [2].

The possible testing methods are limited by many factors, foremost economical feasibility. HCF-testing is time-consuming. For a single test, on the order of 10^7 cycles are required and a large number of tests are needed to get statistically reliable results. Furthermore, to obtain multiaxial stress states, the testing equipment is often complex and expensive. Therefore, alternative testing methods that can be performed on conventional testing machines available at GAS are primarily sought. Another aspect is manufacturing of test specimens. Complex geometries will be more costly to manufacture with the tight tolerances required.

2

Methodology

The workflow of this thesis project is shown in Figure 2.1. This schematic is to a large extent also represented in the structure of the report.

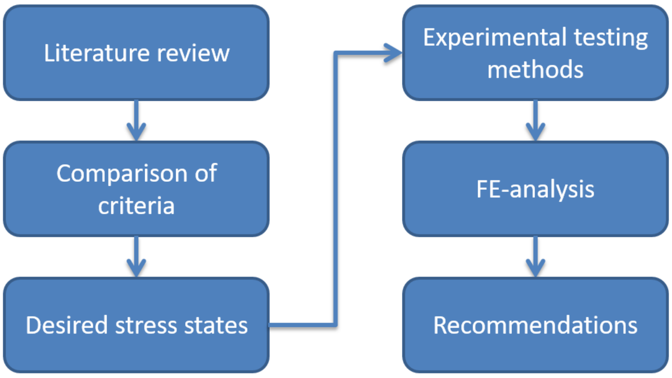

Figure 2.1: Schematic of the project work flow.

First, a literature review was conducted to gain insight in general multiaxial fatigue evaluation. Comparative studies of different criteria were of special interest. As a guidance, a literature review performed at GAS was used [2]. In Chapter 3, some selected multiaxial fatigue criteria are discussed. Furthermore, a short introduction to the basics of fatigue with focus on high cycle fatigue is given.

Five of the fatigue criteria identified in the literature review were implemented in a Matlab-program developed by the author. The stress history is assumed to be proportional, and amplitudes and mid stresses are varied in different ways to evaluate the influence on criteria predictions. Stress states with significant differences in predictions were identified. From this analysis, desired stress states in the experimental testing were determined. This part of the thesis is presented in Chapter 4.

Another literature review was conducted to gain insight into existing testing methods, with focus on biaxial stress states. Two commonly used techniques are identified and presented in Chapter 5. Furthermore, different types of testing machines and statistical methods are briefly discussed. The choice of testing machine and statistical evaluation method may be used to reduce the total test time; either through increasing the frequency or by reducing the number of individual tests.

However, the test methods presented in Chapter 5 require complex and expensive equipment, not available at GAS. Therefore, alternative testing methods only using conventional testing machines were desired. Through inspiration from literature and brain storming, additional concepts ideas were generated. Some of these concepts were further modeled through the FE-softwares *Ansys Workbench* and *Ansys Classic*. This gave an indication of their feasibility. For each concept, different geometries and test setups were evaluated. Results are presented in Chapter 6.

In addition to the Matlab-program previously described, the software *hcfcalc* developed at GAS [4] was used to evaluate the different concepts. This program can be used together with a FE-software and facilitates plotting and visualisation of results. Mid and amplitude stress levels can be imported to *hcfcalc* from an FE-model. The fatigue risk is then evaluated according to Findley or Sines criteria and the results can be exported back to the FE-model. The results can be displayed in different ways. For example, the fatigue risk distribution on the specimen geometry can be plotted and the most critical region can be determined. *hcfcalc* also generates diagrams clearly displaying the fatigue risk for each criterion, which can be used to show differences between Sines and Findley.

To conclude the thesis, a comparison of the concepts was performed in Chapter 7. In this chapter, the advantages and concerns for each concept were summarised. This may serve as as a support when the testing method should be chosen. Furthermore, general recommendation regarding calibration of the criteria are also given.

3

Theory

This theory chapter will introduce the reader to the basic concepts within the area of fatigue. Focus will be on high cycle fatigue at multiaxial stress states. The multiaxial criteria that will be investigated and compared later in the thesis are outlined.

Fatigue is a major concern in the design of structural components. Studies show that around 80% of mechanical failures are caused by fatigue [5]. Even though a component experiences stresses well below the static yield stress, failure may still occur if the load is repeated. A typical example is a shaft in rotating bending, where a material point will experience both compression and tension for each revolution.

3.1 Physics of Fatigue

Fatigue damage is caused by cracks forming and growing through the material. Depending on the micro-structure and loading of the material, different mechanisms will drive the crack. When the crack reaches a critical size, the component will break. A short description of the fatigue damage process will be given below, for further details see for example [3] or [6]. The fatigue process can be divided in the following stages:

1. Crack initiation and short crack-growth (stage I)
2. Long crack-growth (Stage II)
3. Final fracture

Note that this is a simplified model, the actual behaviour will be dependent on the material and loading conditions. Not all stages are always present, and the stages may also be overlapping. In the first stage, cracks often initiate as dislocations in the grain. A pile-up of dislocations will form a slip band that grows within the grain. In the grain boundary, the change of crystal plane directions may in some cases cause a crack arrest. Therefore, smaller grain size will often lead to higher fatigue initiation resistance. Other aspects will also affect, such as the amount of precipitates, impurities and inclusion. This stage is generally shear stress driven, when the crack grows in mode II and/or mode III. The crack direction will be globally oriented 45° from the loading direction in a uniaxial test, as can be seen in Figure 3.1.

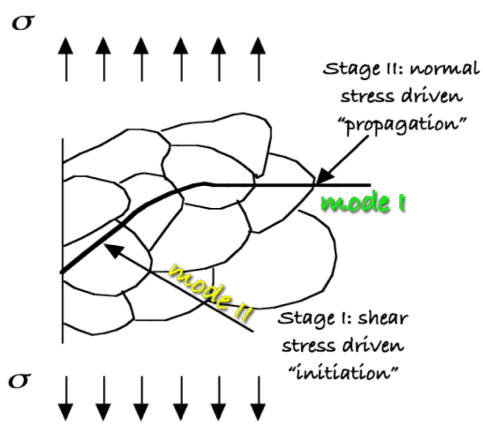

Figure 3.1: Stage I and stage II crack growth, driven by shear stress and normal stress respectively. Taken from [6].

In the second stage, the crack is large enough to create its own plasticity and will grow in mode I. The crack growth will be driven by the maximum tensile stress, which means that it will grow perpendicular to the applied load under uniaxial conditions. This can be seen in Figure 3.1.

In the last stage, a critical size is reached and the stress intensity at the crack tip equals the fracture toughness of the material. The component will fracture. Typical fracture surfaces are shown in Figure 3.2a and 3.2b.

Which of the stages that play the dominant role and constitutes the larger fraction of the fatigue life is dependent on the micro-structure and loading of the material. Generally, in high-ductile materials such as low-carbon steel, the first stage will constitute most of the fatigue life. Hence, the fatigue life is mainly controlled by the cyclic shear stress. On the other hand, materials with internal defects, such as cast iron, mainly experience stage II crack-growth. The defects can be seen as already developed cracks, eliminating stage I crack growth. Therefore the maximum normal stress will be controlling fatigue life.

3.2 High Cycle Fatigue

Fatigue damage is often divided into Low Cycle Fatigue (LCF) and High Cycle Fatigue (HCF). There are no distinct definition separating them, but in the HCF regime deformations are mostly elastic whereas in LCF, plastic deformations are significant and have to be accounted for in the analysis. This means that HCF occurs at lower load levels and longer lives, often when the numbers of cycles to failure are above 10^4.

In the HCF regime, the material fatigue life can often be characterized by a Wöhler-curve (sometimes called SN-curve) showing the magnitude of the cyclic stress against number of cycles to failure. In Figure 3.3, curve A represents a typical steel. In the region from 10^3 to 10^7, data from fatigue testing often falls close to a straight line, meaning that there is a exponential relation between the stress amplitude and cycles

(a)

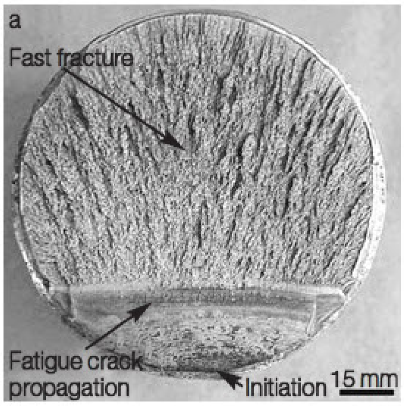

(b)

Figure 3.2: Fatigue crack growth and final fracture of a (a) rail, picture courtesy Anders Ekberg, and (b) shaft, taken from [7].

to failure. For fatigue lives less than $10^3 - 10^4$, i.e. LCF regime, the Wöhler-curve is generally not valid, since plastic deformations are not negligible.

Some metals possess a fatigue limit (also called endurance limit) meaning that stresses below this level can be applied without causing fatigue failure. This corresponds to a knee in the Wöhler-curve for a fatigue life of around $10^6 - 10^7$ cycles. Curve A in Figure 3.3 represents this behaviour. Often in structural design, the aim is to keep the cyclic stresses below this limit. At least theoretically, this will lead to infinite life. However, research [8] shows that this may not be a valid assumption since the curve continues to decrease slowly at very long lives, $10^8 - 10^9$. This is called Very High Cycle Fatigue (VHCF). Furthermore, not all metals possess a fatigue limit. This is for example the case for aluminium alloys, copper and brass where the SN-curves continue to drop [9]. This is represented by curve B in Figure 3.3.

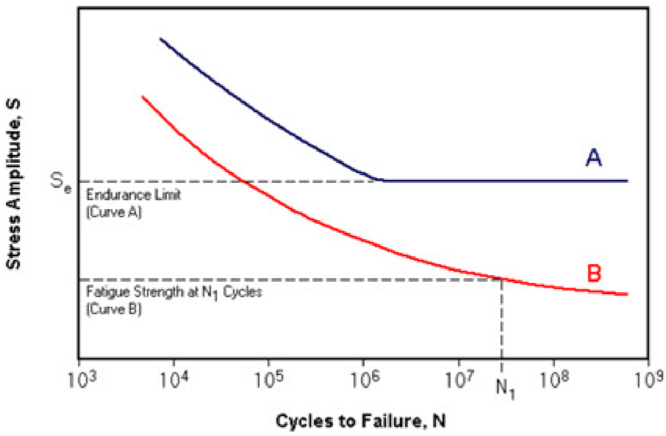

Figure 3.3: A typical Wöhler-diagram for two different materials, material A with a distinct endurance limit. Taken from [10].

3.3 Mid Stress Effects

The effect of a static mid stress on the fatigue life can be displayed in a Haigh diagram, see Figure 3.4a and 3.4b. The curve is drawn for a given number of cycles to failure, N_f, or for the fatigue limit. The mid stress is plotted on the x-axis and amplitude stress on the y-axis. Note that mid stress is sometimes referred to as the mean stress. However, since it is defined as $\sigma_\mathrm{m} = (\sigma_\mathrm{max} - \sigma_\mathrm{min})/2$, it is not an average over time and therefore the term mid stress is more appropriate.

A static tensile stress will have a negative influence on fatigue life, caused by the crack opening effect. If instead the static mid stress is compressive, this will generally lead to a longer fatigue life. However, there are uncertainties partly because experimental data is limited. Therefore, the fatigue life is often assumed to be constant for $\sigma_\mathrm{m} < 0$. This is however not the case in this report.

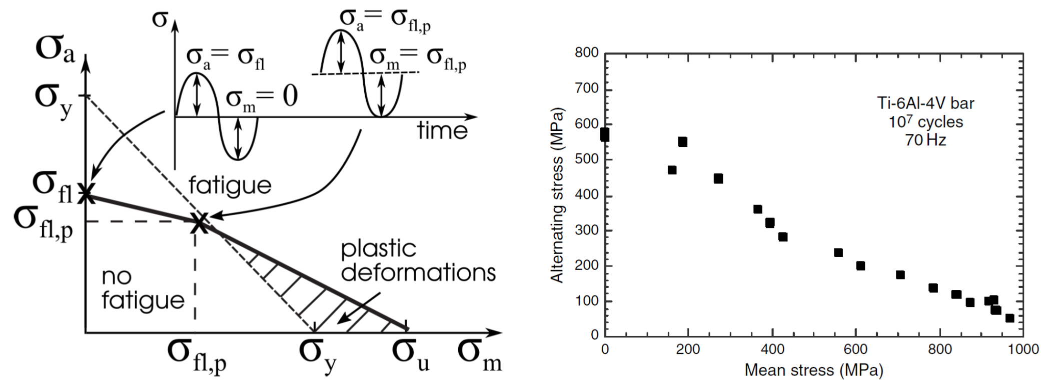

(a) (b)

Figure 3.4: (a) Schematic of a Haigh diagram and (b) constructed from test data for a titanium alloy. Taken from [6] and [10] respectively.

3.4 Multiaxial Fatigue Criteria

Real life components are usually subjected to a complex, three-dimensional state of stress. To be able to compare a general stress state with the fatigue limit obtained from uniaxial testing, a multiaxial fatigue criterion is used. The general state of stress is then reduced to a scalar value, called equivalent stress σ_eq. If this number is below a certain magnitude, σ_e, no fatigue initiation will occur. This means that the uniaxial safe stress range, i.e. stresses below the fatigue limit, is extended to a domain in the multidimensional stress space.

In this thesis, the loading is assumed to be proportional. This means that the stress state as a function of time can be described as:

$$\bar{\sigma}(t) = \begin{bmatrix} \sigma_{m,xx} & \sigma_{m,xy} & \sigma_{m,xz} \\ \sigma_{m,yx} & \sigma_{m,yy} & \sigma_{m,yz} \\ \sigma_{m,zx} & \sigma_{m,zy} & \sigma_{m,zz} \end{bmatrix} + \begin{bmatrix} \sigma_{a,xx} & \sigma_{a,xy} & \sigma_{a,xz} \\ \sigma_{a,yx} & \sigma_{a,yy} & \sigma_{a,yz} \\ \sigma_{a,zx} & \sigma_{a,zy} & \sigma_{a,zz} \end{bmatrix} sin(\omega t) \tag{3.1}$$

Or with symbolic notation:

$$\bar{\sigma}(t) = \bar{\sigma}_{\mathrm{m}} + \bar{\sigma}_{\mathrm{a}} sin(\omega t) \tag{3.2}$$

Where the total stress is divided into a static mid stress tensor, $\bar{\sigma}_{\mathrm{m}}$, and an alternating stress tensor, $\bar{\sigma}_{\mathrm{a}}$.

Existing multiaxial fatigue criteria can be categorized in many ways. One way is according to the following [2]:

- Invariant based criteria
- Critical plane criteria
- Integral plane criteria

For each category, the complexity increases and so do the computational demands. The invariant criteria are based on the first and second invariant of the stress tensor, which makes them easy to compute and evaluate. The mid stress effect is usually measured through the hydrostatic pressure (1st stress invariant), either as the maximum value or mid value during a cycle.

In the critical plane approach, the criterion is evaluated for each plane and the most damaging plane will be limiting. Usually, the maximum shear stress combined with the normal stress on the specific plane is used to assess the fatigue risk. Since all possible planes have to be evaluated, these types of criteria are more computationally expensive. The integral plane criteria add yet another complexity, since the damage parameter has to be integrated over all planes and then the sum is used as a measure of the fatigue risk.

In this thesis, the major focus will be on the currently used invariant criterion (Sines) and the proposed critical plane criterion (Findley). Additionally, three other criteria are included to add extra information in the comparison of criteria. The considered criteria and their evaluation expressed for proportional loading are presented in Table 3.1.

Table 3.1: Fatigue criteria and their evaluation.

Criteria	Category	Evaluation
Sines [11]	Invariant	$\sigma_{eq,S} = \sigma_{vM,a} + c_S\, \sigma_{h,mid} \leq \sigma_{e,S}$
Crossland [12]	Invariant	$\sigma_{eq,CL} = \sigma_{vM,a} + c_{CL}\, \sigma_{h,max} \leq \sigma_{e,CL}$
Manson–McKnight [13]	Invariant	$\sigma_{eq,M} = \sigma_{vM,a}^{1-c_M} (\beta\, \sigma_{vM,m} + \sigma_{vM,a})^{c_M} \leq \sigma_{e,M}$
Dang Van [14]	Critical plane	$\sigma_{eq,DV} = \tau_{Tr,a} + c_{DV}\, \sigma_{h,max} \leq \sigma_{e,DV}$
Findley [15]	Critical plane	$\sigma_{eq,F} =^{max}_{all\ planes} (\tau_a + c_F\, \sigma_n) \leq \sigma_{e,F}$

Where σ_{vM} is the von Mises effective stress (2nd stress invariant of the deviatoric stress tensor), τ_{Tr} is the Tresca effective stress ($(\sigma_1 - \sigma_3)/2$) and σ_h is the hydrostatic pressure ($-(\sigma_1 + \sigma_2 + \sigma_3)$). For further details on the evaluation of each criteria, refer to [11]–[15].

Some comments on the above criteria:

- The parameters c_i and $\sigma_{\mathrm{e},i}$ for each criterion are calibrated from material data. Two data points are needed, for example at different R-values in uniaxial testing or through a combination of uniaxial and torsion test.
- The parameter c_i can be interpreted as the normal stress sensitivity for the invariant criteria. For greater values of c_i, the static mid stress will have larger influence. This is often the case in brittle metals or in materials with initial defects such as cavities, pores, inclusions etc. These defects initiate fatigue cracks early and stage II crack growth are dominating fatigue life [16]. For the Findley criterion the parameter similarly indicates the influence of the normal stress compared to shear stress for the material.
- Even though Dang Van is classified as a critical plane criterion, it can in proportional loading be easily evaluated from the principal stresses. In contrast, the Findley criterion requires that a finite number of planes are considered, which is more computationally expensive.

4

Comparison of Fatigue Criteria

In the following chapter, the fatigue criteria are compared at different states of stress. Regions in stress space where large differences appear can be identified and this will be of great importance when choosing the appropriate testing method. Main focus will be on the comparison of the Sines criterion, currently used in HCF design method at GAS, and the Findley criteria proposed to replace Sines. The other criteria are included to give a broader picture and show general trends. As mentioned earlier, only proportional loading will be regarded.

The evaluation is done through a software developed by the author. As input, the mid and amplitude stress tensors, $\bar{\sigma}_{\mathrm{m}}$ and $\bar{\sigma}_{\mathrm{a}}$, are given and the total stress can be expressed as:

$$\bar{\sigma}(t) = \bar{\sigma}_{\mathrm{m}} + SF\,\bar{\sigma}_{\mathrm{a}} sin(\omega t) \tag{4.1}$$

Through an iterative process, the software will determine the scaling factor SF of the amplitude stress tensor corresponding to the endurance limit for each criterion, i.e. $\sigma_{\mathrm{eq},i} = \sigma_{\mathrm{e},i}$, according to Table 3.1. The scaling factor is a normalised quantity, plotted on the y-axis in some of the diagrams presented later in this chapter.

To calibrate the criteria parameters c_i and $\sigma_{\mathrm{e},i}$, uniaxial test data for a titanium alloy (Ti-6Al-4V) is used [17]. The exact numbers presented in the diagrams below will of course depend on the material. However, results for another material (low-ductile steel) were also produced. The major trends were the same also for this material.

4.1 Stress States

4.1.1 Uniaxial Stress State

For the uniaxial case, the shape of the curves differs only slightly. Sines, Dang Van and Crossland will be equal; represented by a straight line in the Haigh diagram, while Findley is concave and Manson–McKnight convex. The behaviour can be seen in Figure 4.1. Note that the curves coincide for the two test points used for calibration.

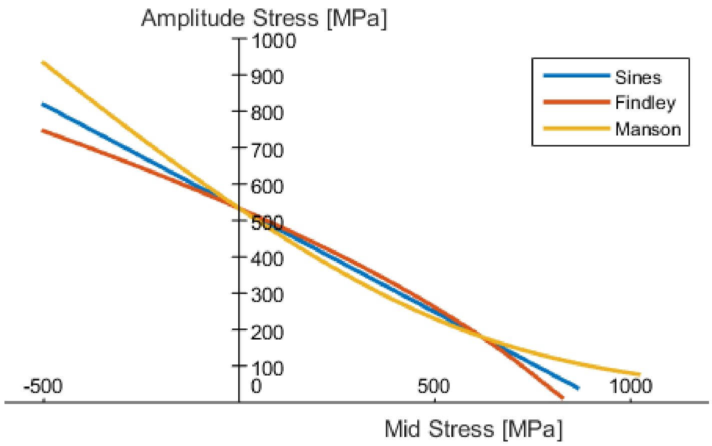

Figure 4.1: Criteria compared at uniaxial stress state. Dang Van and Crossland are equal to Sines and therefore not included.

4.1.2 Equi-biaxial Stress State

As a first indication of how the criteria handle multiaxiality, the uniaxial diagram from Figure 4.1 is reproduced at a equi-biaxial stress state, meaning that the two first principal stresses are equal in magnitude. Both mid and amplitude stresses are equi-biaxial, i.e. $\sigma_{1,m} = \sigma_{2,m}$ and $\sigma_{1,a} = \sigma_{2,a}$. The resulting plot is shown in Figure 4.2, which can be interpreted as a biaxial Haigh diagram.

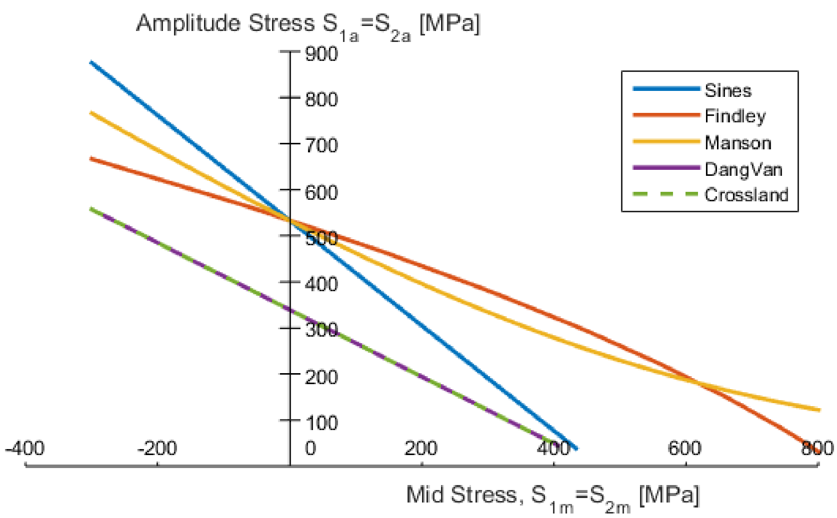

Figure 4.2: Criteria compared at equi-biaxial stress state.

With focus on Sines and Findley, the relative conservatism of Sines for tensile mid stresses is obvious. This tendency will be more pronounced with increasing mid stresses. The difference comes from the way mid stresses are accounted for in the criteria. In Sines, the hydrostatic pressure is used as a measure of mid stress, whereas Findley uses the normal stress on the critical plane. For increasing biaxial mid stresses, the hydrostatic pressure will increase faster than the maximum normal stress, meaning that Sines will give more conservative predictions compared to Findley.

Another observation is the relative conservatism of Dang Van and Crossland. Even though these criteria are similar to Sines at first sight, the use of maximum hydrostatic pressure and not the mid value as in Sines will affect the predictions largely. In this case the equi-biaxial amplitude stress will cause Dang Van and Crossland to be more conservative relative the other criteria, whereas the contrary would be the case if the amplitude would be in shear, i.e. $\sigma_{1,a} = -\sigma_{2,a}$.

4.1.3 Plane Stress State

The stress state at free surfaces can be described as plane stress, since there is no stress component normal to the surface. Then, the proportional stress as a function of time can be described by the principal stresses as:

$$\bar{\sigma} = \begin{bmatrix} \sigma_{1,m} \\ \sigma_{2,m} \\ 0 \end{bmatrix} + \begin{bmatrix} \sigma_{1,a} \\ \sigma_{2,a} \\ 0 \end{bmatrix} sin(\omega t) \tag{4.2}$$

To display possible plane stress states, two non-zero principal stresses are used on the x- and y-axis respectively. Through a variation of the stress state according to Figure 4.3, a comparison of fatigue criterion will be done.

There are different ways to measure the multiaxiality of a stress state. Here the so called triaxiality factor TF will be used to facilitate the comparison of criteria. It is defined as:

$$TF = \frac{3\sigma_h}{\sigma_{vM}} = \frac{\sigma_1 + \sigma_2 + \sigma_3}{\sigma_{vM}} \tag{4.3}$$

In Figure 4.3, different states of stress and the corresponding values of TF is listed.

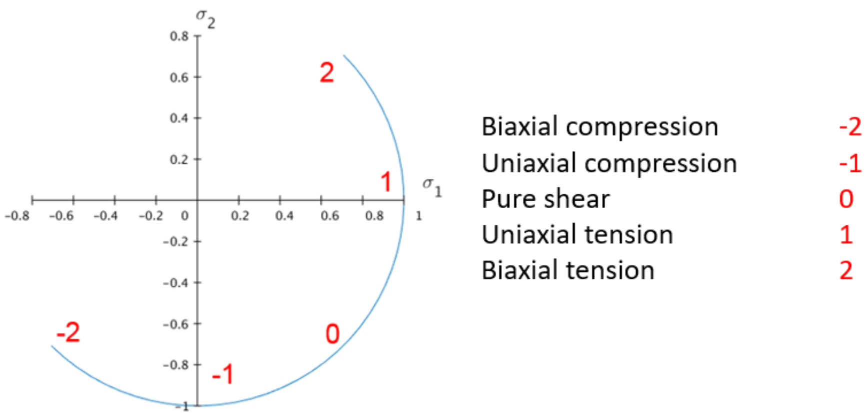

Figure 4.3: Variation of stress state under plane stress condition and corresponding value of TF.

4.1.4 Influence of Mid Stress State

In the following comparison, the mid stress state is altered so that values of TF ranging from -2 to 2 is obtained. The scaling factor SF of the amplitude stress at different TF-value is evaluated and plotted in Figure 4.4. The amplitude is assumed to be biaxial, i.e. $\sigma_{1,a} = \sigma_{2,a}$.

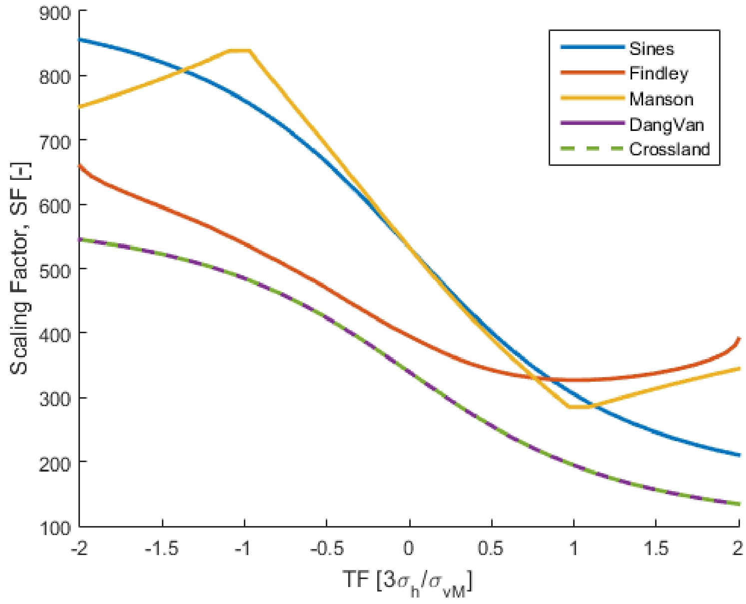

Figure 4.4: Influence of different mid stress states.

For uniaxial tension, i.e. $TF = 1$, one may expect that all criteria would coincide but this is not the case since the amplitude is biaxial and not uniaxial. However, for Sines and Findley the prediction overlap close to $TF = 1$. For values of $TF > 1$, corresponding to biaxial tension, Sines will be more conservative. This is in line with the previously presented results in Figure 4.2. On the other hand, for values of $TF < 1$ (shear- and compressive mid stresses), Findley is more conservative.

4.1.5 Influence of Amplitude Stress State

An additional comparison was performed by varying the stress state of the amplitude, while assuming no mid stresses. This analysis showed no significant differences between Sines and Findley. For more details, see Appendix A.

4.1.6 Influence of Mid Stress Direction

A critical plane criterion like Findley will be sensitive to the direction of the mid stress compared to the direction of amplitude stress. Direction in this context means that both mid stress and amplitude stress are individually uniaxial, but can be applied in different directions. A simple numerical example can be used to illustrate this. Assume a uniaxial mid stress in direction 1: $\sigma_{1,m} = 600\,\text{MPa}$. For Sines, there will be no difference if the amplitude is applied in direction 1 or any other direction, the allowed amplitude will still be the same: $\sigma_a = 190\,\text{MPa}$. But for Findley, the critical plane and its normal stress will differ depending on direction. If applied in the same direction, the allowed amplitude is close to the prediction of Sines: $\sigma_a = \sigma_{a,1} = 190\,\text{MPa}$. If instead applied perpendicular to the mid stress, the allowed amplitude is significantly higher: $\sigma_a = \sigma_{2,a} = 357\,\text{MPa}$. The above example is illustrated in Figure 4.5.

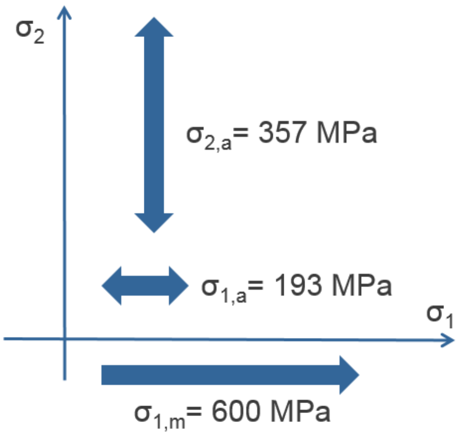

Figure 4.5: Illustration of numerical example showing the influence of mid stress direction captured by Findley.

4.2 Calibration of Criteria Parameters

An important aspect when comparing the criteria is the calibration of parameters. Calibration points should be chosen close to the actual stress state in the component, or in this case the test specimen, to gain best results. For example, if shear stresses are dominating, test data from torsion tests are probably more suitable. From an economical point of view, material data that is already available are of course preferable to use. At GAS, most material data are from uniaxial testing at different R-ratios. Parameter calibration for the presented testing methods are further discussed in Chapter 7.

The considered criteria contain two parameters, so that two calibration points are required. For the investigated material, test data was available for several different R-ratios in uniaxial testing. Therefore, different pairs of test points could be chosen and how this affected the parameters c_i and $\sigma_{\mathrm{e},i}$ was briefly investigated. There were significant differences for all criteria, and as high as 40 % for some criteria. Therefore, it can be concluded that all criteria are sensitive to the choice of calibration points. This further stress the importance of calibration.

To be able to say anything about the robustness of the different criteria, further investigation with test data from different materials and stress states must be conducted. This was not within the scope of this project.

4.3 Main Conclusions

From the above analysis, some states of stress are of special interest. These are listed below. The first two are illustrated in Figure 4.6, whereas the third is illustrated in Figure 4.5. Once again it is noted that the focus is mainly on Sines and Findley, and stress states where these two criteria differ.

1. Mid stress in biaxial tension, i.e. in the first quadrant of Figure 4.6. For this state of stress, Sines is conservative compared to Findley, especially for high mid stresses.
2. Mid stress in shear, i.e. principal stresses with opposite signs, corresponding to the second quadrant. Findley is conservative compared to Sines.
3. Uniaxial mid stress with amplitude stress in different direction, as illustrated in Figure 4.5. Critical plane criteria can predict an influence of mid stress direction, in contrast to invariant criteria.

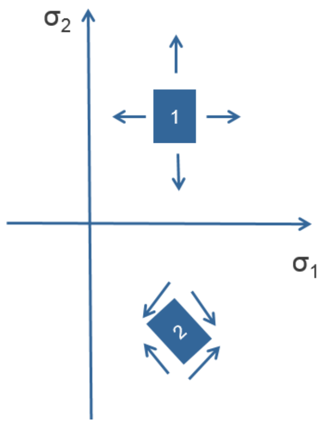

Figure 4.6: Illustration of stress states that are of extra interest.

Among them, the first stress state is chosen for testing. The reason is:

- This is a stress state often present in the engine components, especially for rotating parts subjected to HCF.
- Current design methods using Sines criterion appear to be overly conservative in this stress state. Even though the mid stress is well below the biaxial yield limit, no stress amplitude is allowed, see Figure 4.2. This seems unrealistic from an engineering point of view.

Hence, the investigation of possible testing methods will only focus on specimens and test setups that generate a stress state with tensile biaxial mid stresses.

5

Common Biaxial Testing Methods

This chapter will give an overview of common testing methods found in the literature. Three aspects are of interest; specimen geometry, testing equipment, and method for evaluating the fatigue limit. Only test setups generating a biaxial tensile stress state will be presented. Good and thorough description of multiaxial testing techniques in general can be found in [18] and [19].

5.1 Test Specimens

Through a literature review, it was apparent that two types of specimens are most commonly referenced. These are the tubular specimens and the cruciform specimens, displayed in Figure 5.1.

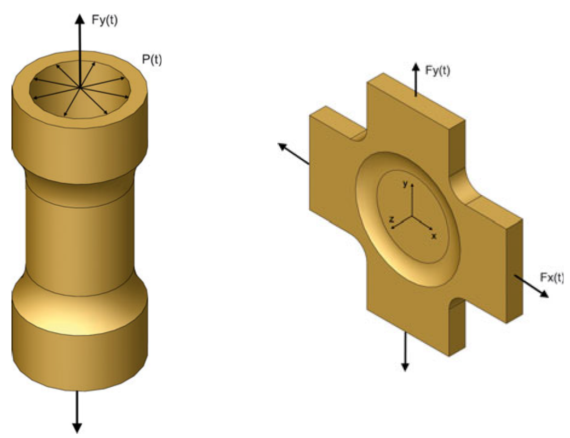

Figure 5.1: Example of biaxial test specimens. Left: tubular specimen with internal pressure. Right: cruciform specimen loaded in four arms. Taken from [20].

5.1.1 Cruciform Specimen

The cruciform specimen is loaded in two directions to create a biaxial stress state in the middle region. Often, this region has a reduced thickness to assure failure. Two independent load system are used and stress states in all four quadrants are possible to achieve (compare Figure 4.6). However, there is a risk of buckling when the specimen is loaded in compression. There are commercial biaxial machines available on the market, but these are quite rare compared to conventional uniaxial equipment. The cruciform specimen is used mainly for static strength testing, but fatigue tests have been conducted. Testing in the HCF regime are not common but can be found, see for example [21].

The main challenge with this geometry is to assure that fatigue will initiate in the intended region. The specimen has to be carefully designed in the region where the arms meet. Examples of geometrical design can be seen in Figure 5.2. As mentioned, the center region is often reduced in thickness to concentrate stresses. However, this introduces stress gradients and a homogeneous stress field is hard to achieve. Several reports can be found on the optimization of cruciform specimens, for example [22] and [23]. Another drawback is that the stress in the specimen can not be calculated directly from the applied loads, but has to be obtained from an FE-analysis.

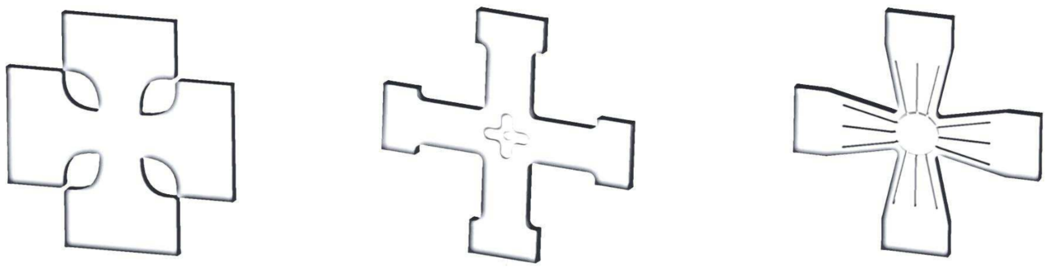

Figure 5.2: Example of geometrical designs of cruciform specimen, from [23].

5.1.2 Tubular Specimen with Internal Pressure

Tubular specimens are quite commonly used for multiaxial testing. Combined loading in different ways are possible, for example torsion/tension, torsion/bending and internal pressure/tension. However, only the latter will produce a biaxial stress state in tension (1st quadrant in Figure 4.3).

For the tubular specimen with combined internal pressure and tension, two independent load systems are required. To achieve a close to homogeneous stress field, the wall thickness has to be small compared to the diameter. If so, the radial stress can be neglected compared to hoop and axial stresses. Furthermore, the variation of hoop stress through the thickness will be small, generating a large volume of material that will be uniformly stressed. The stress state can easily be calculated from the applied loads with simple, analytical equations.

Among the drawbacks are the risk of buckling when the thin walled specimen is loaded in compression. Additionally, when the internal pressure is high there is a risk for bulging walls which will alter the obtained stress state. Examples of combined internal pressure/tension experiments conducted with tubular specimen can be found in [24]–[28]. Figure 5.3 is taken from [24] and shows a broken specimen.

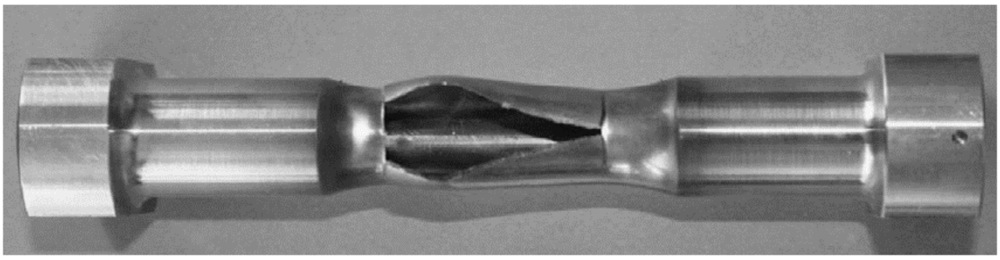

Figure 5.3: Tubular specimen with internal pressure, cycled to failure. Taken from [24].

5.2 Comparison

A summary of advantages and concerns for the two testing methods are given in Table 5.1. Both test methods require two independent load systems. Furthermore, the test frequencies are often low. This together means time consuming and costly experiments. At GAS, the equipment required for these kinds of tests is not available. Therefore, alternative methods that could be performed on conventional testing machines are sought and will be presented in the next chapter.

Table 5.1: Summary of advantages and concerns for the two commonly used biaxial testing methods.

Specimen	Advantages	Concerns
Cruciform specimen	• Flexible loading, all quadrants and R-ratios possible • In-plane loading	• FE-analysis required to determine stress state • Non-uniform stress field and stress gradients • Assure failure in test region • Strain measuring difficult in test region
Tubular specimen with internal pressure	• Uniform stress distribution • Stress state easily calculated • Easy strain measurement	• Risk for bulging walls • Risk for buckling

5.3 Testing Machines

The most widely used equipment for fatigue testing is uniaxial hydraulic machines, shown in Figure 5.4a. The frequency is typically in the range from 1–30 Hz. Alternative machines have been proposed to increase testing frequency, for example electro-dynamic shakers, shown in Figure 5.4b, and ultrasonic testing devices. Common for these machines are that they work near the resonance frequency of the specimen, so-called vibration based fatigue testing.

(a) **(b)**

Figure 5.4: (a) Hydraulic fatigue testing machine and (b) electro-dynamic shaker used for vibration based testing. Taken from [29] and [30] respectively.

5.3.1 Vibration Based Fatigue Testing

The most commonly used machine for vibration based fatigue testing is the electro-dynamic shaker. The test specimen is excited close to its natural frequency, often in the range 300–3000 Hz. The increase in test frequency compared to conventional hydraulic machines will significantly reduce test times. Another advantage is that less forces is needed to generate the desired stress field, reducing power consumption. Furthermore, the change in frequency response of the specimen throughout the test can be used as a measure of damage accumulation. Examples of experiments performed with electro-dynamic shakers can be found in [31] and [32].

Another machine that can be used for vibration based fatigue testing is the ultrasonic testing device. It comprises a generator, a piezoelectric transducer and an ultrasonic horn. The frequency is typically around 20 kHz. For more details about this testing technique, see [33]. At such high frequencies, there is a risk of heating of the specimen. Pauses in the testing are regularly taken to avoid temperature increase.

Vibration based techniques has mainly been used for uniaxial loading but examples of multiaxial fatigue testing can be found in the literature. George et al [31] used a plate with a geometry that produces biaxial bending when excited in a electrodynamic shaker. However, the experimental results are limited and no conclusions regarding the reliability of the testing technique can be drawn. Furthermore, Vieira et al [34] present experimental results from multiaxial loading using an ultrasonic testing device. Through the design of the ultrasonic horn, both axial and torsional modes are induced in the test specimen at the same frequency. Limited test data are available, and the reliability of the test method cannot be judged.

In vibration based testing, the control of frequency and amplitude is important to obtain the desired stress levels. For an outline of how experiments are controlled, see Section 6.2.3.

5.4 Methods for Evaluation of Fatigue Limit

Beside the test frequency and the number of cycles, the total test time is also dependent on the number of tests required to obtain the material properties of interest. In the HCF regime, an estimate of the mean and standard deviation of the fatigue limit is often the main purpose. One commonly used method is the staircase method which will be briefly described. Furthermore, the step testing method is presented as an example of an accelerated testing technique. However, several other methods exists and for further details see for example [35] and [36].

5.4.1 Staircase Testing

The staircase method was introduced by Ransom and Mehl [37], in an attempt to shorten testing times. The method is widely used nowadays. The stress level for each test is determined from the previous test. If the previous specimen failed, the stress levels is reduced by one step or, if the specimen was unbroken, the stress level is increased one step. The step size is usually predefined, as well as the number of cycles defining the endurance limit, often $10^6 - 10^7$. A schematic diagram of a staircase test series is shown in Figure 5.5.

5.4.2 Step Testing

Conventional testing methods, like the staircase method, still require a lot of time consuming tests which is prohibitive for many investigations [10]. This has led to the search for abbreviated statistical methods. One of them are the step testing technique, described in [38]. For each test specimen, the stress is increased in steps. Starting at a level below the expected fatigue limit, the specimen is subjected to a given number of cycles, often $N_{life} = 10^7$. If the specimen survives a block of 10^7 cycles, the stress level is increased by a certain step (around 5%). This is done until failure occurs. The fatigue limit can then be determined using a linear interpolation:

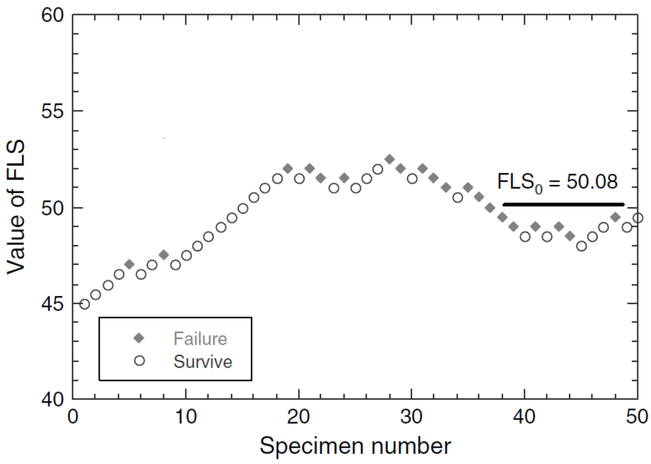

Figure 5.5: Example of staircase testing series, from [10]. FLS is denoting Fatigue Limit Strength, equivalent to endurance limit.

$$\sigma_e = \sigma_0 + \Delta\sigma \left(\frac{N_{fail}}{N_{life}} \right) \tag{5.1}$$

Where σ_0 is the previous stress level that did not result in failure, $\Delta\sigma$ is the step size and N_{fail} are the number of cycles to failure at stress level $\sigma_0 + \Delta\sigma$. The validity of the step testing method may be questionable, since specimens are reused at increasing stress levels. This is done under the assumption that stresses below the endurance limit are not damaging for the material. However, as mentioned earlier, the existence of an endurance limit is not evident for all metals. With this said, Nicholas [38] shows good validation of the method for step testing performed on a titanium alloy (Ti-6Al-4V).

6

Alternative Testing Concepts

The testing techniques presented in the previous chapter require two independent load systems which make the equipment complex and expensive. Furthermore, the testing frequency is often low. Hence, the experiments are often costly and the available testing machines are limited [21]. Alternative testing methods that can be performed on conventional testing machines are therefore sought. The available equipment at GAS are uniaxial hydraulic testing machines and electro-dynamic shakers.

The test method must be able to create a biaxial mid stress, an alternating biaxial amplitude around a zero mid stress is not enough. Several concepts were generated with inspiration from literature, combined with own ideas and input from others. Four concepts were taken on for further analysis:

- *Disc bending*, where a disc shaped specimen is loaded transversely in a hydraulic testing machine.
- *Vibrating disc*, where a disc shaped specimen is pre-loaded in a fixture and then excited near resonance frequency by a electro-dynamic shaker.
- *Hourglass specimen*, where a uniaxial load creates a biaxial stress state in a test region in the middle of the specimen. A hydraulic testing machine is used.
- *Shrink fit of tubular specimen* onto an over-sized shaft to create internal pressure, and axial load applied in a hydraulic testing machine.

The analyses for the concepts were carried out with material data from a titanium alloy, Ti-6Al-4V. If the biaxiality in the test region is 1, i.e. $\sigma_1 = \sigma_2$, desirable stress levels [MPa] for testing purpose are:

$$\bar{\sigma} = \begin{bmatrix} \sigma_{1,m} \\ \sigma_{2,m} \\ 0 \end{bmatrix} + \begin{bmatrix} \sigma_{1,a} \\ \sigma_{2,a} \\ 0 \end{bmatrix} sin(\omega t) = \begin{bmatrix} 450 \\ 450 \\ 0 \end{bmatrix} + \begin{bmatrix} 200 \\ 200 \\ 0 \end{bmatrix} sin(\omega t) \tag{6.1}$$

At this mid stress level almost no amplitude is allowed according to Sines, whereas Findley allows around 350 MPa. This can be seen in Figure 4.2. If this stress state can be generated, the testing method will be able to clarify what criterion is most accurate.

To visualise the difference in Sines and Findley fatigue predictions, *hcfcalc* is used. This is a software developed at GAS to evaluate multiaxial HCF. The main output from the program is the utilization factor UF, representing the fraction used of the limit effective stress:

$$UF = \frac{\sigma_{\text{eff},i}}{\sigma_{\text{lim},i}} \tag{6.2}$$

Note that $\sigma_{\text{eff},i}$ corresponds to $\sigma_{\text{eq},i}$, and $\sigma_{\text{lim},i}$ equals $\sigma_{\text{e},i}$ using the notation in Table 3.1. The UF-magnitude is illustrated graphically in a Limit diagram for the Findley criterion in Figure 6.1.

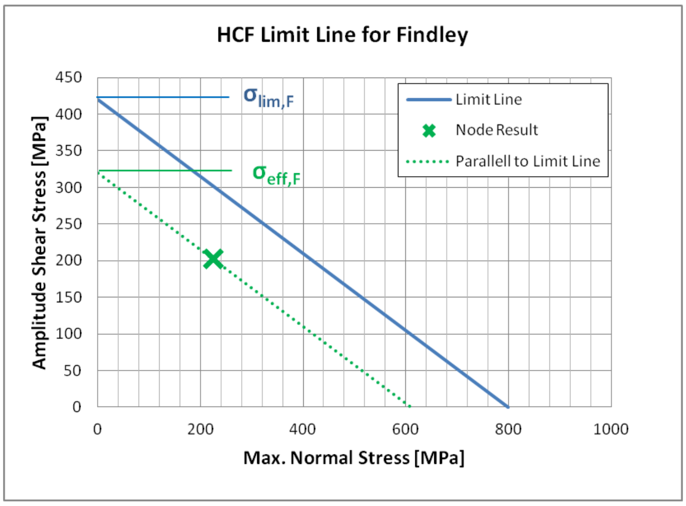

Figure 6.1: Example of Limit diagram from *hcfcalc* for the Findley criterion, from [4].

The program is integrated into an FE-analysis of the test specimen loading. The mid and amplitude stresses for each node in the model are exported from the FE-analysis to *hcfcalc* and fatigue evaluation is performed. The results are then imported back to the FE-program where UF-magnitudes are displayed graphically in the post-processing. Additionally, limit diagrams (as the one shown in Figure 6.1) are used to visualise the difference in criteria predictions. In these diagrams, results from each node in the FE-model is represented by a point. For points above the limit line, the stresses are above the fatigue limit according to the considered criterion. Note that for Findley, the x-axis corresponds to the maximum normal stress on the critical plane and y-axis shows shear stress amplitude in the critical plane. This is different from the figures in Chapter 4 where mid and amplitude stresses were shown on the respective axes.

6.1 Disc Bending

The disc bending concept is a biaxial version of three- or four-point bending. A disc is supported at its edges, and a load is applied in the middle region to cause a biaxial bending stress state. The load can be applied either through a load ring or as a point load in the middle. The two concepts are illustrated in Figure 6.2a and 6.2b respectively. The first concept is used by Koutiri et al [39] for HCF testing of cast aluminium. The second concept is used by Brugger et al [40], where the load is applied through an ultrasonic device. A similar concept is the pressurised disc fatigue (PDF) technique, where the load is instead applied from a cyclic pressure, see [41] and [42].

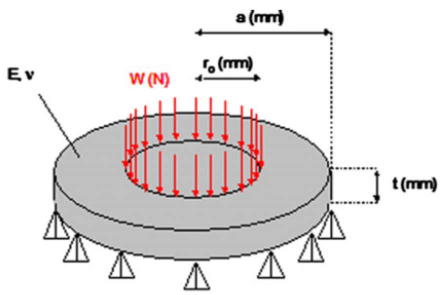

(a)

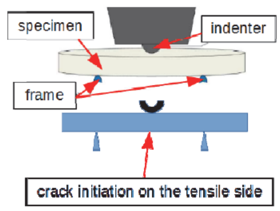

(b)

Figure 6.2: Two versions of disc bending, using (a) load ring, illustration from [39] and (b) point-load, illustration from [40].

The stress state will vary through the thickness of the plate, with tensile stresses on the lower surface and compressive stresses on the upper surface. Hence, cracks will initiate on the lower surface. Depending on how the load is applied, different stress distributions will be generated in the plate. With a point load, the stresses will be at maximum in the middle and then decrease towards the edge. If a load ring is used, the entire area inside the load ring will experience the maximum stress, see Figure 6.4. Testing is limited to positive R-ratios, since the arm is only pushing on the disc.

6.1.1 Stress Uniformity

The stress distribution in the plate is evaluated through FE-analysis. The results presented are for a disc with diameter of 200 mm and a thickness of 5 mm. The load ring has a diameter of 50 mm and a rounded edge that bear against the specimen. The radial stress is plotted in Figure 6.3. It is seen that maximum tensile stresses occurs on the lower surface in the middle region.

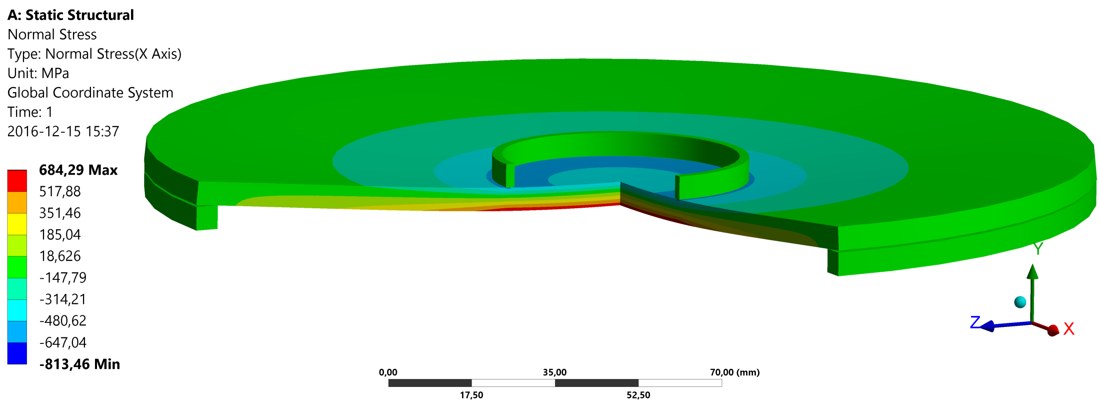

Figure 6.3: Radial stress distribution in the disc, subjected to a total load of 20 kN.

The stress distribution is shown in Figure 6.4, where radial and hoop stress are plotted for the lower surface, from the center point and towards the support. As can be seen, the stress is almost uniform within the load ring, and then drops towards zero at the support.

Figure 6.4: Radial stress (A) and hoop stress (B) plotted along the lower surface, from centre of plate towards the support.

It is noted that large deformations has to be accounted for in the FE-model to capture membrane effects. If the load is applied through a load ring, there will be a stress concentration on the lower surface of the disc below the ring. This can be seen in Figure 6.4, where the radial stress increases approximately 5 % from the value in the centre of the disc. This stress concentration is explained by the localised deformation close to the load ring and will be more pronounced for a thinner disc. An analogy with a drum skin can be made, where deformation only occurs around the support and leaves the rest of the skin flat.

The stress should be as uniform as possible. Thus, the stress concentration caused by this effect should be reduced. One way is to increase the thickness of the disc. However, a thick disc will require more load to generate the desired stress state. For this geometry (5 mm radius and 200 mm thickness), a transverse force of approximately 20 kN is needed to obtain desired stress levels ($\sigma_1 = \sigma_2 = \sigma_{max} = \sigma_m + \sigma_a = 650$ MPa). This is well within the range of most hydraulic testing machines. The corresponding variation of stress around 5 % at the ring is considered to be acceptable.

6.1.2 Control of Experiment

One way to calibrate specimen and machine is to use strain gauges on the test specimen. These can be mounted in the middle region on the upper surface to monitor stresses during the experiment, without influencing crack development. The stress levels are then calibrated against the FE-model. Another way is to use one test specimen dedicated for calibration only, where the strain gauges can be mounted in the actual test region. This will ensure that the correlation between applied force and stress obtained from the FE-model is correct.

In uniaxial bending, e.g. four-point bending, a crack will significantly influence the stiffness of the specimen. Therefore, the measured deflection can be used to detect cracks and as a definition of failure. There will likely not be that clear relation for the disc bending, since the structure is more stiff. Even for a large crack in the disc, there is still a great amount of remaining material that carries the load. A small investigation of the crack influence on stiffness was done and the results are summarised in Table 6.1. The crack modelling is done through FE-analysis, where an elliptical edge crack is assumed. The crack depth is 2.5 mm, i.e. half of the disc thickness, and the crack length is varied to see its influence on stiffness and natural frequency.

Table 6.1: Crack influence on stiffness and natural frequency of a disc with 200 mm diameter and 5 mm thickness. Crack depth is 2.5 mm and the total length of the crack is given.

	Center Deflection	Natural Frequency
No crack	2.59 mm	1242 Hz
Crack length 20 mm	2.63 mm	1238 Hz
Crack length 40 mm	2.68 mm	1233 Hz

As seen in Table 6.1, there is only a small increase in centre deflection, even for large cracks. On the other hand, there is no preferred crack direction in the test zone. Therefore, it may be more probable that several small cracks will develop, which will affect stiffness and deflection in a different way. Hence, no general conclusion about crack detection can be drawn. Instead, it is recommended to use a first specimen for calibration purposes, from which an appropriate detection method (also considering e.g. optical measurement, eddy current and similar methods) can be determined.

6.1.3 Shear Stress in the Contact Stress Field

For this testing technique, it is important to assure that the load application ring will not initiate failure. There will be shear stresses induced locally in the specimen, as well as potential fretting in the interface. However, results show that with enough thickness this should not pose a problem. In Figure 6.5, shear stresses are plotted for the same load level as displayed in Figure 6.3 and 6.4. The contact surface on the load ring has a radius of 10 mm and a friction coefficient of 0.2 is assumed. As can be seen, the maximum levels are close to the contact on the compressive side, where the risk for fatigue cracks growing large is very small. Furthermore, the magnitude is relatively small, which suggests that cracks will not initiate from the contact region. Note that the risk is also depending on the geometry of the load ring. An optimization of the geometry in the contact region should reduce the shear stresses even further.

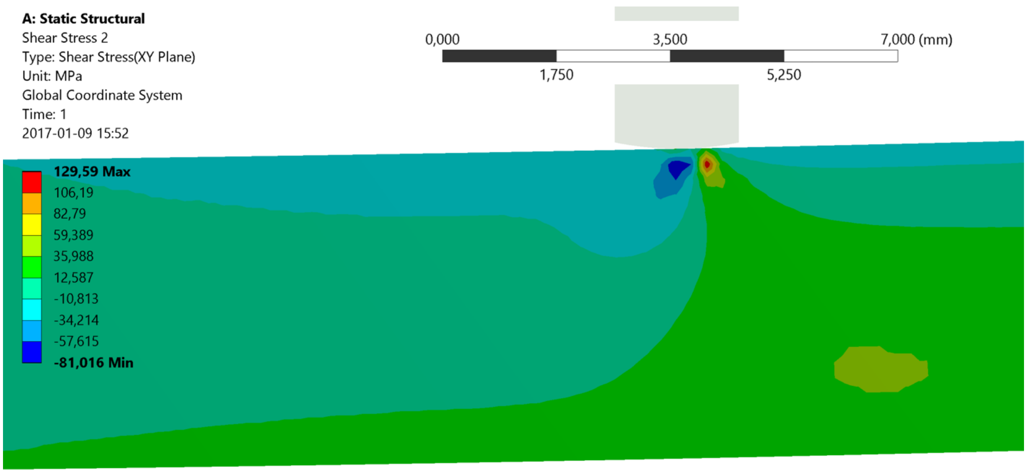

Figure 6.5: Shear stress distribution close to the load application from a 2D-axisymmetric model. A friction coefficient of 0.2 in the contact interface is assumed.

6.1.4 Criteria Comparison

The ability to differentiate between criteria is manifested by the limit diagrams for the Sines and Findley criteria. There are significant differences as can be seen in Figure 6.6. The stress levels in the test region correspond to the ones given in Equation 6.1.

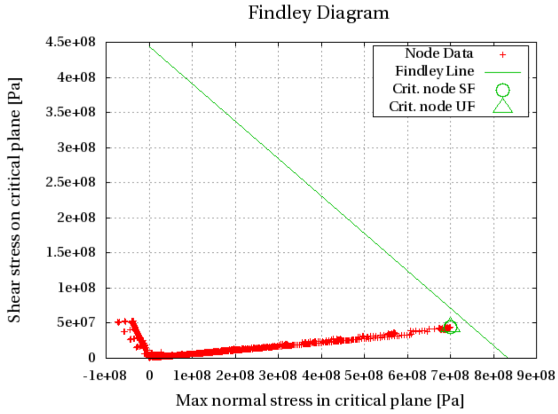

(a)

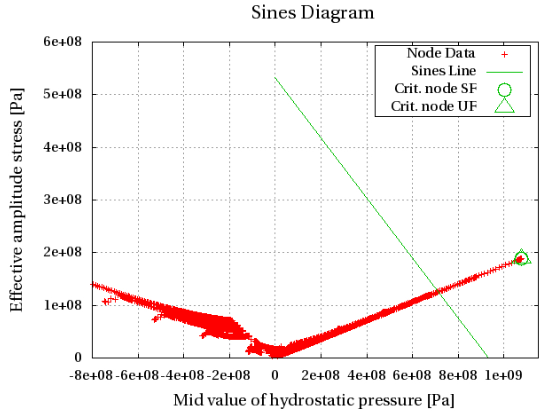

(b)

Figure 6.6: Limit diagrams from *hcfcalc* for the Disc bending-concept evaluated by Findley and Sines criteria respectively.

6.2 Vibrating Disc

This concept is based on a disc shaped specimen excited near its resonant frequency in an electro-dynamic shaker. The main advantage is the shortened test times. The test frequency is often around 300–1500 Hz, depending on specimen geometry. Compared to using a conventional hydraulic testing machine working around 20 Hz, the test time to accumulate 2×10^6 cycles can be reduced from 27 hours to less than 2 hours.

A general problem with vibration based testing techniques is how to achieve a mid stress, i.e. testing at an R-value different from $R = -1$. In this concept, static mid stresses are imposed on the disc through a fixture. Then, the disc is excited in its first vibrational mode, causing a biaxial bending stress state. The first vibrational mode for a disc with clamped edges is illustrated in Figure 6.7.

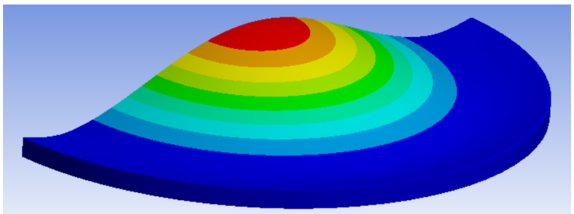

Figure 6.7: Half model of the first vibrating mode for a disc with clamped edges.

6.2.1 Pre-stress in Fixture

Different ways of achieving the mid stress have been considered, either as in-plane tension or out-of-plane bending. Note that these methods are only conceptual and further analysis is required to evaluate their feasibility.

- The disc will be heated onto an oversized fixture, similar to the shrink fit of the tubular specimen in Section 6.4. An edge on the outside circumference of the disc will grip around the fixture, illustrated in Figure 6.8. When the disc is cooled down to room temperature, residual stresses will be imposed. The region where the disc is attached to the fixture must be carefully designed, firstly to avoid stress concentrations and secondly to reduce the bending moment induced on the disc.
- The disc will be tighten onto the fixture through equally spaced screws around the circumference. Through measuring on the disc surface, the strain field can be monitored and the tightening of the screws can be tuned to obtain a homogeneous stress field with desired magnitude. The measuring can be done either using strain gauges or by digital imaging technique. It will also be important to assure that no relaxation occurs during vibration.

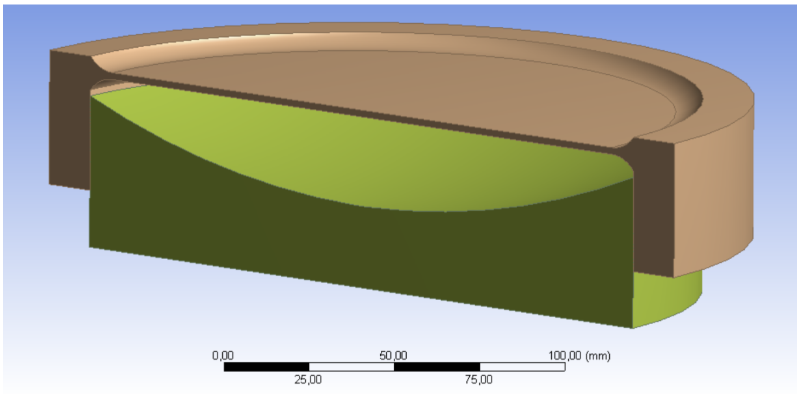

Figure 6.8: Half model showing how the static mid stress can be imposed by shrink fitting the specimen onto an oversized fixture.

- Another way of creating the static mid stress is to use a fixture causing the plate to bend. The idea is illustrated in Figure 6.9. The disc is bent like a bowl. It is important that an even curvature is achieved.

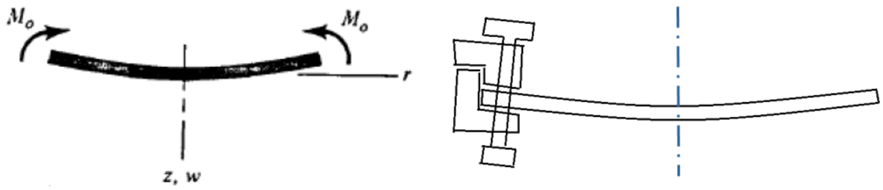

Figure 6.9: Illustration showing pre-bending in a fixture with inclined edges to bend the disc like a bowl. This will create static mid stresses.

6.2.2 Stress Distribution and Criteria Comparison

With this testing technique, the obtained stress state will be a combination of static pre-stress and vibrational stress. The pre-loading from the fixture, either pre-tension or pre-bending, are evaluated through a static FE-analysis. In a second step, the harmonic response is evaluated using a modal analysis where the pre-stress from previous analysis is included. The pre-stress significantly affects the natural frequency of the disc, as well as the obtained vibrational stress state. Preferably, both mid stress and amplitude stress should reach its maximum in the same region of the specimen, which will be the intended test region.

For results from these analyses, see Appendix C. It turned out to be hard to find good combinations of pre-stress and vibrational stress. Despite several concepts with different geometry and loading, no satisfactory solution was found. The concept that showed the most promising results is presented in Figure 6.10.

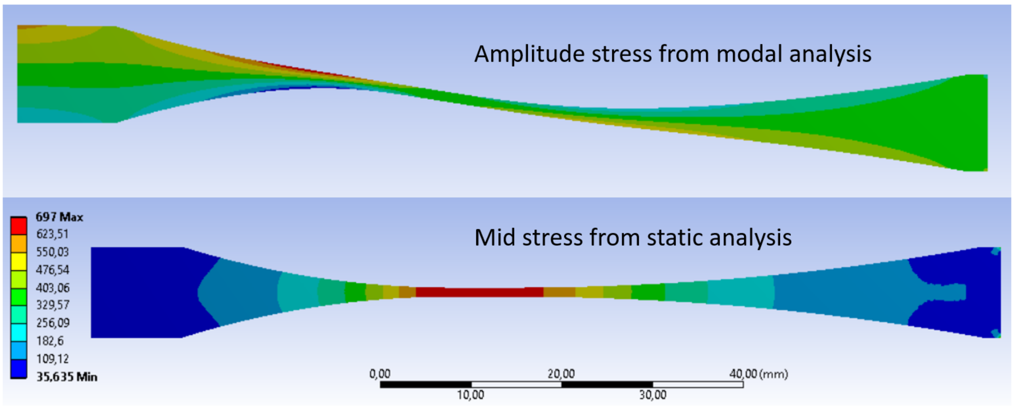

Figure 6.10: Radial stress distribution for mid- and amplitude stress for a 2D-axisymmetric model of the disc. The symmetry axis is along the left edge of the geometry.

The disc has a nominal thickness of 10 mm in the centre and around the circumference. A gradual reduction of thickness is used to concentrate stresses, and the minimum thickness is 1 mm. In Figure 6.10, the radial stress is shown. The hoop stress will have almost the same distribution but smaller in magnitude. As can be seen, mid and amplitude stress will not have the same distribution and maximum magnitude will occur in different regions. However, better results may be achievable through an optimization of the geometry.

The utilization factor UF according to the Findley criterion is shown in Figure 6.11. This represents the fatigue initiation risk across the disc. The employed pre-stress corresponds to Figure 6.10, and the amplitude stress is scaled so that the most critical node has $UF = 1$.

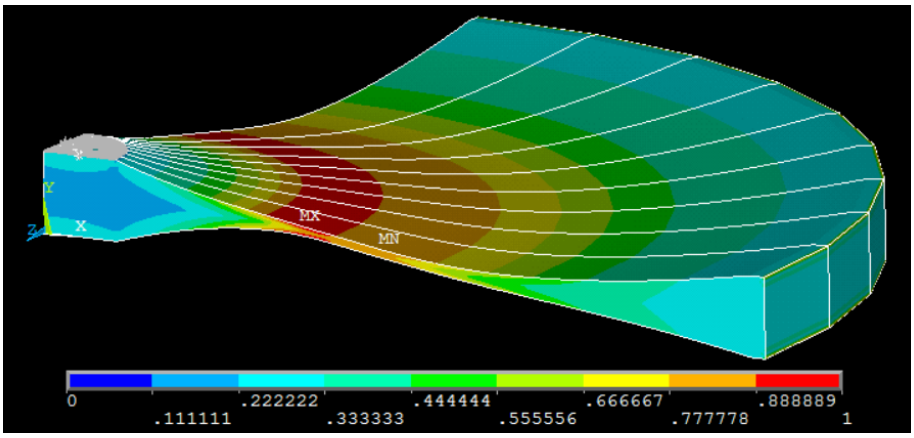

Figure 6.11: Utilization factor UF according to the Findley criterion, showing the fatigue initiation risk.

For the magnitude of pre-stress suggested in Figure 6.10, the Sines criterion will be more conservative than Findley, as can be seen in Figure 6.12a and 6.12b. Sines is actually predicting that no amplitude is allowed for a great portion of the disc (each point corresponds to a node in the FE-model). This proves that the testing concept should be able to compare the accuracy of the two criteria.

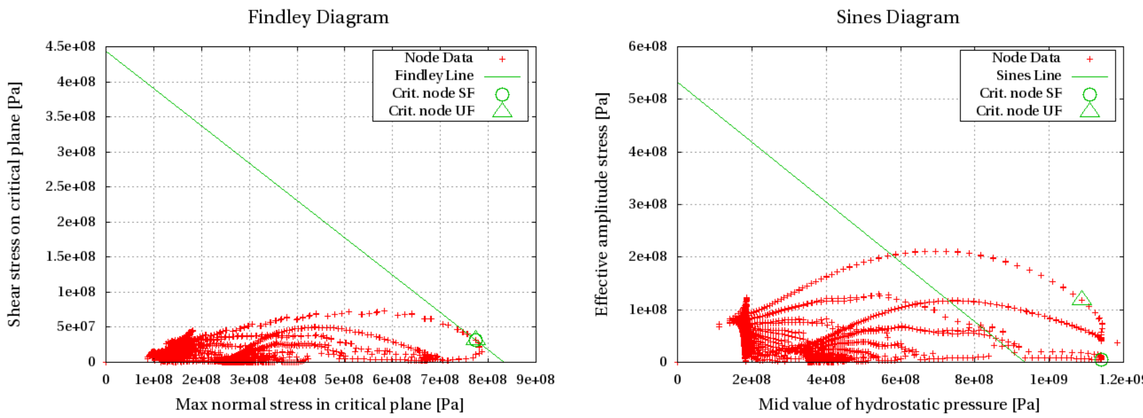

(a) **(b)**

Figure 6.12: Limit diagrams from *hcfcalc* for the Vibrating disc-concept evaluated by Findley and Sines criterion respectively.

To lower the resonant frequency, weights can be added in the middle region of the disc. For the geometry in the concept above, a weight of 0.5 kg is added and the resulting frequency with pre-tension is approximately 500 Hz. At this frequency, the displacements and velocities are sufficiently large for easy measuring. If the operational frequency is higher, the accuracy of measuring devices tends to decrease.

6.2.3 Control of Vibration Based Testing

When running a vibration based fatigue test, the control of the frequency and amplitude are of great importance. The test is usually conducted in the following way:

- Find proper specimen geometry so that the desired resonant mode and its frequency are within the working range of the shaker. This is usually done through FE-analysis.
- As a first part of the calibration, mount the specimen on the shaker and perform a frequency sweep to find the natural frequency of the system. This should be close to the one computed.
- As a second part of the calibration, a relationship between shaker amplitude and stress level in the specimen are sought. The shaker amplitude during the test is usually monitored by an accelerometer and for the desired stress level, a setpoint should be determined. If possible, strain gauges are mounted in the test region so that the actual stresses can be determined during calibration. The strain gauges may then be removed during testing.
- Perform the test, adjusting the frequency so that the setpoint of the accelerometer is kept. A secondary measure, for example a laser measuring the deflec-

tion, can also be employed to assure that the desired stress level is kept.

- When the frequency drop is larger than a certain percentage, the specimen has reached a limit determined for failure and the test is stopped.

A schematic illustration of the control system used in [32] is shown in Figure 6.13. The accelerometer is used as the primary control measure, and a laser vibrometer monitors the deflection during the test.

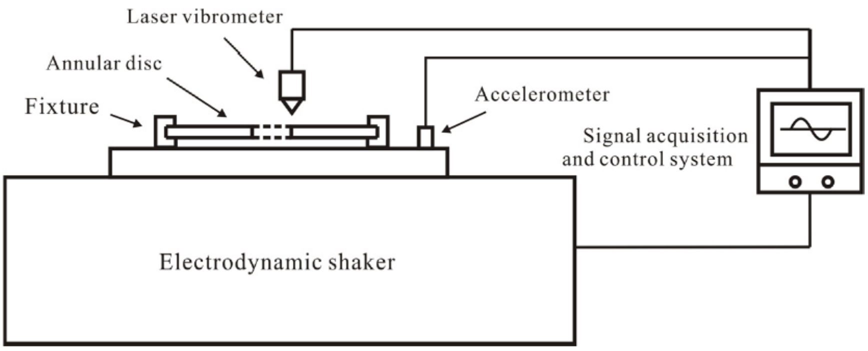

Figure 6.13: Schematics showing the control system for vibration based fatigue testing used in [32].

Regarding the last step, the frequency drop may not be a good measure of failure for this concept since the stiffness of the disc is not that sensitive for cracks. Even for a crack of significant length and depth, there is still a great amount of undamaged material carrying load. The investigation in Section 6.1.2 seems to confirm this hypothesis, since the frequency drop in Table 6.1 is very small. This suggests that crack detection can be a concern also for this testing method.

6.3 Hourglass Specimen

The purpose of this concept is to create a biaxial stress state in the specimen through an applied uniaxial force. A conventional hydraulic testing machine can be used. The biaxiality is created by an hourglass shaped geometry, in which the axial load will also pull the test section in transverse direction, see Figure 6.14.

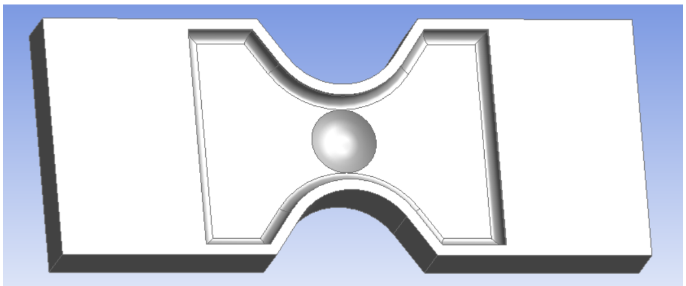

Figure 6.14: Proposed test specimen that creates biaxial stress state in the test region.

The following should be taken into account when designing the specimen:

- The stress state in the test region should be as uniform as possible, keeping the gradients close to the middle region as low as possible.
- The volume of material experiencing maximum stress should be as large as possible.
- The fatigue initiation should occur in the test region, and not at other critical locations. For example, the outside radius may also be critical as shown in Figure 6.15b. This should be evaluated through a fatigue analysis, and a certain overloading should be achieved for the test region compared to elsewhere in the specimen.
- To be able to differ between the fatigue criteria (Sines and Findley), the biaxiality ratio should be at least 0.4, where there are significant differences for high mid stresses.
- The specimen should fit in an ordinary hydraulic testing machine. The maximum width of the specimen is set to 45 mm to be mountable in the grips.

Some of the items above are contradicting and the geometry will be a trade-off. A manual iteration loop has been performed to find a suitable geometry. However, by using an optimization algorithm better results are probably achievable.

A similar hourglass concept was used by Bellett et al [20], displayed in Figure 6.15a. However, this specimen geometry showed to be inappropriate. For a cast material containing internal defects, the failure occurred at the outside radius as shown in Figure 6.15b. In this region the normal stress will reach its maximum value. For materials where fatigue is mostly related to normal stress, this will be the critical region for crack initiation. However, in the proposed specimen, the maximum normal stress occurs in the test region as can be seen in Figure 6.16. At the same time, a similar biaxiality ratio is kept: $(\sigma_1/\sigma_2 = 0.4)$. Therefore, this specimen geometry seems more promising for testing, also for brittle materials.

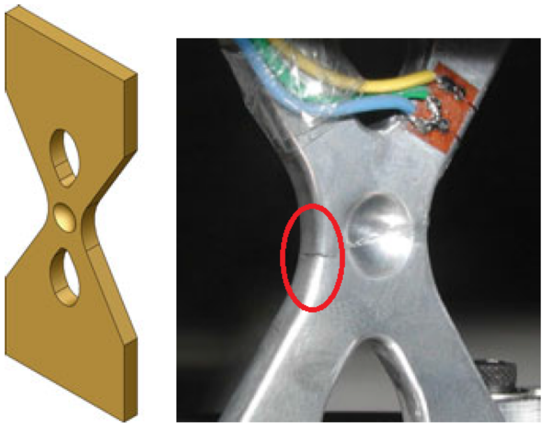

(a) **(b)**

Figure 6.15: Specimen used in [20], (a) showing geometry and (b) cracks initiating from the outside radius and not in the test region.

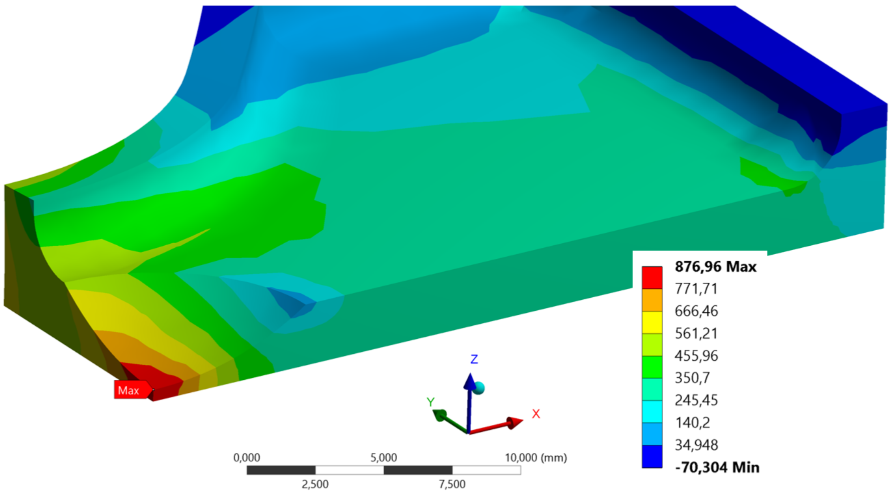

Figure 6.16: 1/8-model of the geometry showing longitudinal (x-direction) stress distribution in the specimen, with maximum magnitude in the test region.

6.3.1 Fatigue Initiation and Stress Uniformity

The specimen geometry is analysed using FE-simulations. The applied axial force is $F = 31.5 \pm 14.5$ kN, corresponding to R=0.4. In Figure 6.17, the fatigue initiation risk is assessed with the Findley criterion for a titanium alloy (Ti-6Al-V4). In the test region, the utilization factor UF is 1.2, in other areas the maximum is 0.9. This means a ratio of 1.3 between these regions, which should be sufficient to assure that fatigue failure occurs in the test region.

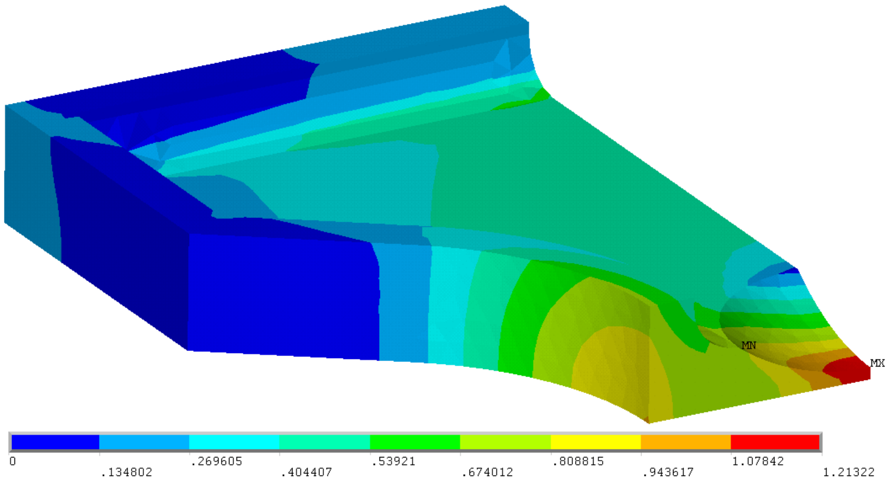

Figure 6.17: 1/8-model of the geometry showing *UF*. Values above 1 indicates a stress level above the endurance limit according to the Findley criterion.

Figure 6.18 shows the stress distribution through the thickness in the centre point of the specimen. No major variations can be seen. Figure 6.19 shows how the stress decreases quite rapidly out from the test region in both transverse and longitudinal direction. This means that only a small volume of material is experiencing maximum stresses. However, a greater volume and a higher uniformity is hard to achieve without increasing size of the specimen.

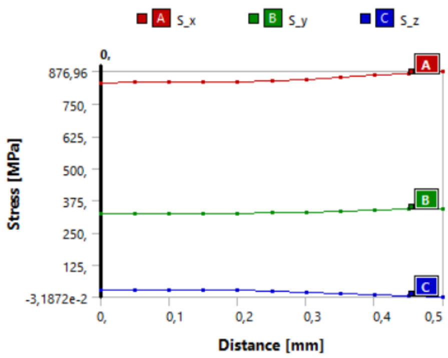

Figure 6.18: Stress components (σ_x, σ_y and σ_z) through the thickness of the test region, 0 mm corresponding to middle of test specimen and 0.5 mm the surface. See coordinate system in Figure 6.16.

6.3.2 Control of Experiment

Strain measuring in the test region is not possible due to the small and curved surfaces. Instead, strain gauges must be placed elsewhere. This imposes an extra degree of uncertainty. As cracks grow in the test region, no significant loss in stiffness can be expected since the thicker material surrounding the test region will be load carrying. Therefore, for a load controlled test, the difference in deflection may not

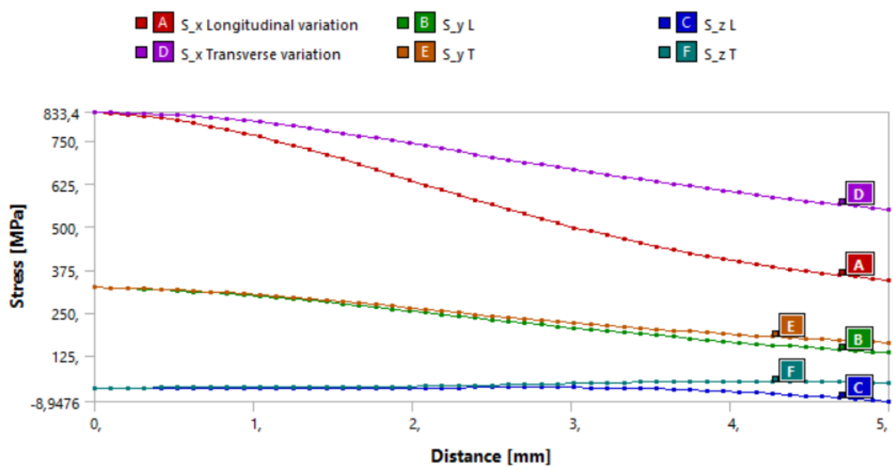

Figure 6.19: Variations of stress components (σ_x, σ_y and σ_z) from middle of test specimen in longitudinal (x) and transverse direction (y). See coordinate system in Figure 6.16.

be large enough to detect cracks. Instead, complementary methods such as eddy current testing, penetrant or surface replicas can be used.

6.3.3 Criteria Comparison

For the suggested geometry, a biaxiality of 0.4 is reached. This is above the requirement. For this biaxiality ratio, there will be significant differences between Sines and Findley predictions as can be seen in Figure 6.20. For mid stresses around $\sigma_{1,m} = 600$ MPa and $\sigma_{2,m} = 240$ MPa, the testing method should have a good capability of differentiating the criteria. Principal direction 1 here corresponds to the longitudinal direction and principal direction 2 to the transverse direction.

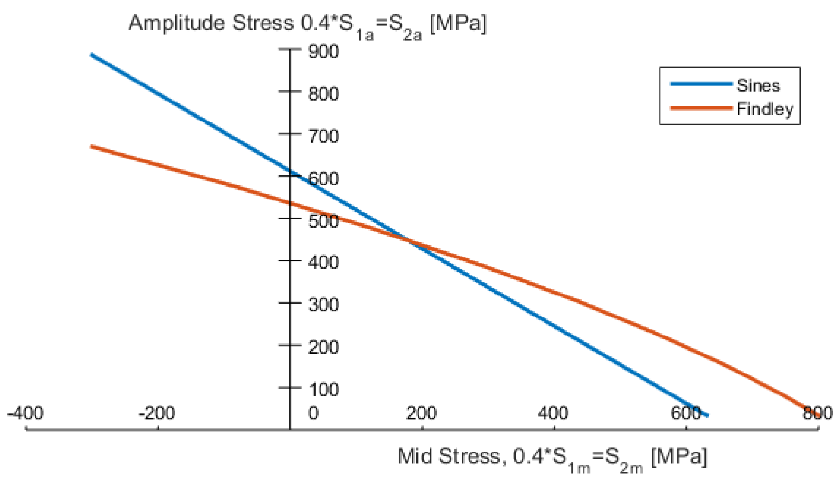

Figure 6.20: Predictions from Sines and Findley criteria for a biaxiality ratio of 0.4.

6.4 Shrink Fit of Tubular Specimen

This concept idea is based on a tubular specimen, where the internal pressure is obtained through a shrink fit onto an oversized solid shaft. The tubular specimen, see Figure 6.21, is heated and will therefore expand. It is also possible to cool the solid shaft in liquid nitrogen to be able to use an even bigger interference. The shaft is then inserted into the hole of the tubular specimen. When the configuration has returned to room temperature, an internal pressure is obtained from the interference.

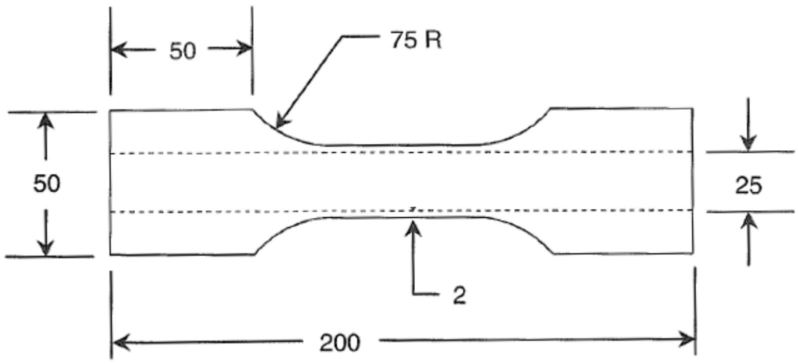

Figure 6.21: Dimensions of tubular specimen used for tension/torsion testing from [3]. This was used as a starting point for the simulations.

The feasibility of the concept is investigated through FE-analyses. The main concerns and requirements when designing the specimen are:

- Avoid fretting in the interface between the tubular specimen and solid shaft. If not, fretting fatigue may shorten the life and test results will not be reliable.
- Cracks should preferably initiate on the outer surface, to facilitate the detection of cracks and to verify that fretting is not influencing the results. Usually, the drop in stiffness is used as a definition of failure. However, since the solid shaft will be load carrying after failure of the specimen, this effect will not be that significant.
- It will no be possible to fully achieve a uniform stress state through the thickness, but a requirement of max 10 % variation is set.

6.4.1 Risk of Fretting Fatigue

As already mentioned, there is a risk of fretting in the interface between shaft and tube. This may in turn cause fatigue cracks to initiate, so called fretting fatigue. Figure 6.22 illustrate the wear rate increasing as a function of slip amplitude in the interface. Furthermore, it can be seen that fatigue life reaches a minimum value and then increases again. This is because cracks initiated in the fretting zone will be worn off, if the slip amplitude is large enough.

To give an indication of the fretting risk, the test setup was evaluated through FE-

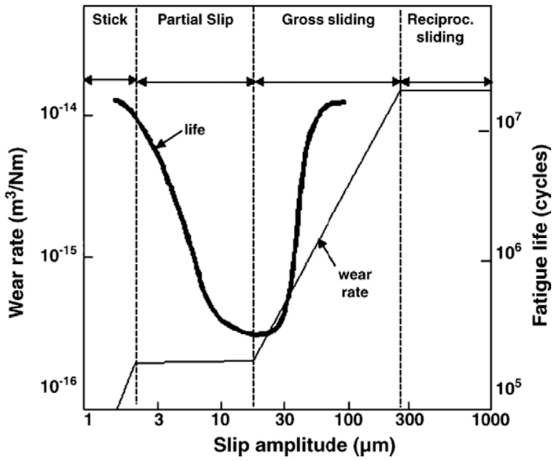

Figure 6.22: Effect of slip amplitude on wear rate and fatigue life, from [43].

simulations. The condition is set that no slippage in the interface between shaft and tube is allowed. The axial force applied in the testing machine will initiate slipping if the magnitude is above a threshold value. On the other hand, certain stress levels must be reached for testing purposes. The simulation will indicate if these levels are reached before slippage occurs. In Appendix D required stress levels together with material properties and additional assumptions can be found.

6.4.2 Simulation Results

As a starting point, a geometry for a typical tubular specimen found in [3] were used, as shown in Figure 6.21. Simulations showed that this was not a suitable geometry, for further details see Appendix D. The critical point is located in the interface, and stress levels are too low when slippage occurs.

Through a manual iterative process, a better geometry was developed. It turned out that only small variations in wall thickness from the test section to the nominal thickness were allowed to avoid slipping. The reason is that strain variations along the tube length will cause relative motion to the solid shaft. The best performing geometry found has a 1.5 mm wall thickness in the test section, whereas the nominal wall thickness is 2 mm. The stress distribution for this geometry is shown in Figure 6.23.

To obtain the critical point on the outer surface, the test section length is shortened and the transition radius adjusted to cause a small stress concentration. The result can be seen in Figure 6.24, where the stress variations through the wall thickness are plotted.

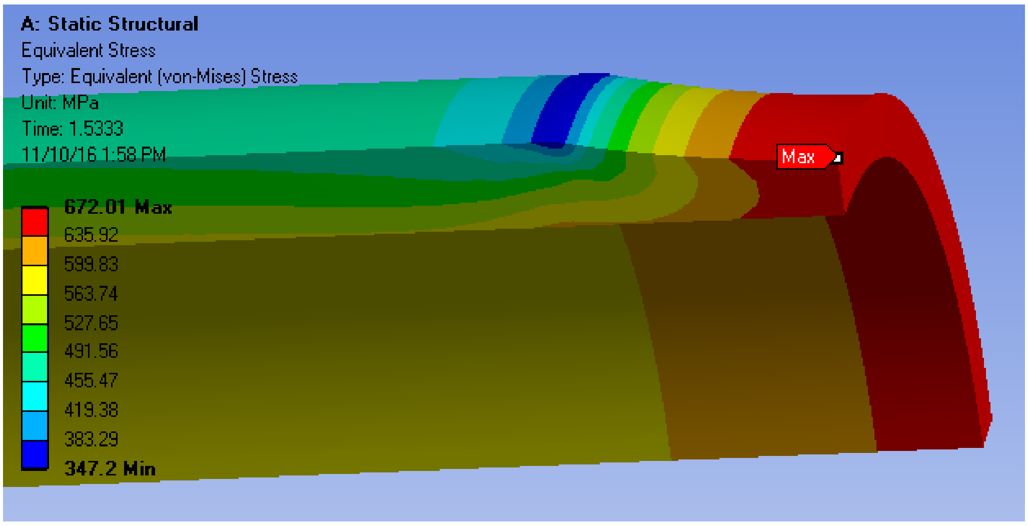

Figure 6.23: Von Mises effective stress distribution for the improved geometry.

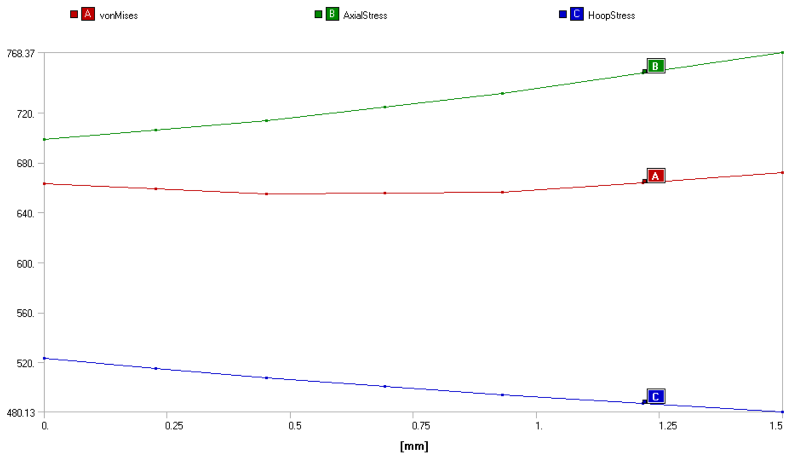

Figure 6.24: Stress variation through wall thickness, axial stress, hoop stress and von Mises effective stress.

The decreasing hoop stress is compensated by an increasing axial stress towards the outer surface. This will result in a close-to-constant effective stress, while at the same time keeping the variations below 10 % as required. The desired stress levels are almost reached. However, there are other concerns with this concept making it non-competitive towards other test methods:

- Manufacturing challenges: For example a long hole with tight tolerances and thin walls.
- Uncertainties caused by the tight tolerances: Small geometrical deviations from nominal design will cause great impact on the obtained stress state. As an example, the stress state is sensitive to variations in transition radius and wall thickness in test section.

6.4.3 Considered Modifications of the Concept

To overcome the problem with cracks initiating from the interface, a concept with two solid shafts were considered, as illustrated in Figure 6.25. A small gap is left in the middle, approximately 2–4 mm, short enough so that the hoop stress will not drop significantly in this region. With this concept, the tubular specimen will carry all load in the gap region in contrast to the concept of a continuous shaft. The following advantages are obtained:

- Much lower axial force has to be applied to reach the desired stress states.
- Failure will be concentrated to the gap region where stresses will be substantially higher than in the rest of the test specimen.
- Crack detection will be facilitated since a distinct drop in stiffness will occur.

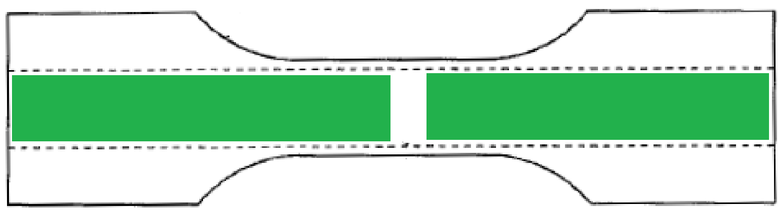

Figure 6.25: Modification of the concept through the use of two solid shafts, illustrated in green.

However, the main drawback is the increased risk of fretting. It is well-known that fretting risk is most severe near a sharp edge. Since only a small gap can be allowed, this critical region will be close to the test region and will most likely influence the fatigue life. Therefore, this concept was dismissed.

7 Conclusions & Recommendations

This chapter will conclude this thesis with a comparison of the concepts, outlining advantages and concerns. The uniaxial calibration possibilities are also discussed. Furthermore, final recommendations regarding choice of concept are given.

7.1 Calibration

An important aspect in the test planning is the calibration procedure, discussed in Section 4.2. In the calibration, material data from uniaxial testing should preferably be used. These tests are well-controlled and provide reliable data. Furthermore, most of the available material data at GAS are from uniaxial testing.

For a fair comparison, the criteria should to an extent as large as possible be calibrated in similar conditions as the test regarding:

- Type of loading, for example in-plane tension or bending.
- Stress gradients and volume effects, due to notches and other geometrical variations.
- Similar mid stress level, i.e. R-value.

The disc bending concept provides good calibration capabilities. The volume of the material in the test region can be chosen by changing the size of the load applying ring. Hence, the biaxial test can be designed to mimic a uniaxial four-point bending test regarding loaded volume. Since both uniaxial and biaxial tests create bending, the stress distribution through the thickness of the specimen will be the same.

In the hourglass specimen, there are stress gradients close to the test region. Furthermore, the volume of material in the test region is small. This together makes it hard to find a similar uniaxial calibration test. The shrink fit concept can be tested uniaxially by removing the internal pressure. The tubular specimen is simply used without the solid shaft. For the vibrating disc concept a uniaxial version may be possible. A beam like specimen with the same thickness variation can be tested in a similar fashion with a electro-dynamic shaker. One end is clamped in the shaker, and the other end is free to vibrate.

7.2 Final Recommendations

Table 7.1 summarises the advantages and concerns for the presented concepts. The disc bending concept is recommended due to its simplicity compared to the other concepts. Reasons to avoid complex geometries, for example varying thicknesses, are:

- Harder to manufacture within tolerances.
- Difficult to model numerically with high accuracy.
- Harder to measure stresses during experiments using for example strain gauges.

The disc bending concept has a simple geometry with constant thickness providing a well controlled stress state. There are less uncertainties compared to the other concepts. This concept also provides good calibration from uniaxial testing as discussed in the previous section.

Table 7.1: Summarising table

Advantages	Concerns
Disc Bending	
• Simple geometry • Good calibration possibilities – similar to uniaxial four-point bending • Almost uniform stress state in a large volume of material	• Design of fixture for load application and support • Only positive R-ratios • Shear stress and fretting from load application
Vibrating Disc	
• Simple geometry • High frequency – shorter test times	• Generating pre-loading through fixture • Frequency change caused by friction/loosening in fixture grip • Non-uniform stress field
Hourglass Specimen	
• Simple to use in conventional testing machine	• Assure failure in intended region • Different geometries for different biaxiality factors • Manufacturing challenges • Stress gradients and volume effects
Shrink Fit	
• Simple to use in conventional testing machine	• Tight tolerances • Manufacturing challenges • Fretting risk

Bibliography

[1] Kaufmann, Markus. "Cost/weight optimization of aircraft structures." (2008).

[2] Brommesson, Rebecka. "VOLS:10221395 – Multiaxial HCF, Literature review." GKN Aerospace Sweden Internal Report (2016).

[3] Socie, Darrell, and Gary Marquis. "Multiaxial fatigue." Warrendale, PA: Society of Automotive Engineers, 1999. 502 (1999).

[4] Högström, Gunnar. "VOLS:10229096 – Program to perform multiaxial HCF analysis, hcfcalc." GKN Aerospace Sweden Internal Report (2016).

[5] Lundh, Hans. "Grundläggande hållfasthetslära." Institutionen för hållfasthetslära, Tekniska högsk. (2000).

[6] Ekberg, Anders. "Multiaxial Fatigue, Edition 5.1." Department of Applied Mechanics, Chalmers Tekniska högsk., (2016).

[7] "Linear Elastic Fracture Mechanics (LEFM): Part Two" http://www.totalmateria.com/page.aspx?ID=CheckArticle&site=KTS&NM=299 (accessed 2016-12-30)

[8] Bathias, Claude. "Relation between endurance limits and thresholds in the field of gigacycle fatigue." Fatigue Crack Growth Thresholds, Endurance Limits, and Design. ASTM International (2000).

[9] Murakami, Yukitaka. "Metal fatigue: effects of small defects and nonmetallic inclusions." Elsevier (2002).

[10] Nicholas, Theodore. "High cycle fatigue: a mechanics of materials perspective." Elsevier (2006).

[11] Sines G., "Behavior of Metals under Complex Static and Alternating Stresses." Metal Fatigue, Sines G. and Waisman J.L. Editors, McGrawHill (1959).

[12] Crossland B., "Effect of Large Hydrostatic Pressures on the Torsional Fatigue Strength of an Alloy Steel." Proceedings of the International conference on Fatigue of Metals, Institution of Mechanical Engineers, London (1956).

[13] Gyekenyesi, John Z., Pappu LN Murthy, and Subodh K. Mital. "Nasalife-Component fatigue and creep life prediction program." (2014).

[14] Dang Van K., "Sur la résistance à la fatigue des métaux." Thèse de Doctorat ès Sciences, Sci.Techniq.l'Armement, 47, 647 (1973).

[15] Findley W.N. "Fatigue of metals under combinations of Stresses." Transactions of the American Society of Mechanical Engineers, vol 79 (1957).

[16] Bruun, Ø. A., and G. Härkegård. "A comparative study of design code criteria for prediction of the fatigue limit under in-phase and out-of-phase tension–torsion cycles." International Journal of Fatigue 73 (2015): 1–16.

[17] Salar, S. and Sandberg, D. "Test data – Statistical evaluation of the test results obtained from uniaxial fatigue tests performed for 12% Cr-steel and Titanium Ti-6-4." TurboPower Deliverable Report, Report No. TVB-D4.3 (2011).

[18] Ziebs, J., et al. "Experimental techniques for testing materials under multiaxial loading." ICBMFF4 (2013).

[19] Makris, A., et al. "A review of biaxial test methods for composites." Experimental Analysis of Nano and Engineering Materials and Structures (2007): 933–940.

[20] Bellett, Daniel, et al. "A Biaxial fatigue specimen for uniaxial loading." Strain 47.3 (2011): 227–240.

[21] Cláudio, R. A., L. Reis, and M. Freitas. "Biaxial high-cycle fatigue life assessment of ductile aluminium cruciform specimens." Theoretical and Applied Fracture Mechanics 73 (2014): 82–90.

[22] Baptista, Ricardo, et al. "Design optimization of cruciform specimens for biaxial fatigue loading." Frattura ed Integrita Strutturale 30 (2014): 118.

[23] Andrusca, Liviu, Viorel Goanta, and Paul Doru Barsanescu. "Optimizing the Shape and Size of Cruciform Specimens used for Biaxial Tensile Test." Applied Mechanics and Materials. Vol. 658. Trans Tech Publications (2014).

[24] Bonnand, V., et al. "Investigation of multiaxial fatigue in the context of turboengine disc applications." International Journal of Fatigue 33.8 (2011): 1006–1016.

[25] Bonnand, V., et al. "Experimental and theoretical comparison of some multiaxial fatigue design criteria in the context of life assessment of rotating parts in turboengines." ICAF 2009, Bridging the Gap between Theory and Operational Practice. Springer Netherlands (2009): 743–764.

[26] Lefebvre, D., et al. "A high-strain biaxial-testing rig for thin-walled tubes under axial load and pressure." Experimental mechanics 23.4 (1983): 384–392.

[27] Gaur, Vidit, et al. "Effect of biaxial cyclic tension on the fatigue life and damage mechanisms of Cr–Mo steel." International Journal of Fatigue 87 (2016): 124–131.

[28] Doquet, Véronique, and Vincent De Greef. "Dwell-fatigue of a titanium alloy at room temperature under uniaxial or biaxial tension." International Journal of Fatigue 38 (2012): 118–129.

[29] Instron. "Instron 8801 (100kN) Fatigue Testing Systems." http://www.instron.se/sv-se/products/testing-systems/dynamic-and-fatigue-

systems/servohydraulic-fatigue/8801-floor-model (accessed 2017-01-10)

[30] Brüel & Kjær. "Brüel & Kjær LDS V875 Medium-force shaker." https://www.bksv.com/en/products/shakers-and-exciters/LDS-shaker-systems/medium-force-shakers/V875 (accessed 2017-01-10)

[31] George, Tommy J., et al. "Development of a novel vibration-based fatigue testing methodology." International Journal of Fatigue 26.5 (2004): 477–486.

[32] Xu, Wei, et al. "Multiaxial fatigue investigation of titanium alloy annular discs by a vibration-based fatigue test." International Journal of Fatigue 95 (2017): 29-37.

[33] Stanzl-Tschegg, Stefanie. "Very high cycle fatigue measuring techniques." International Journal of Fatigue 60 (2014): 2-17.

[34] Vieira, M., et al. "Development of a Very High Cycle Fatigue (VHCF) multiaxial testing device." Frattura ed Integrita Strutturale 37 (2016): 131–137.

[35] Weibull, Waloddi. "Fatigue testing and analysis of results." Elsevier (2013).

[36] Pollak, Randall D. "Analysis of methods for determining high cycle fatigue strength of Ti-6Al-4V gigacycle fatigue behavior." (2005).

[37] Ransom, J. T., and R. F. Mehl. "The statistical nature of the endurance limit." Transactions of the American Institute of Mining and Metallurgical Engineers 185.6 (1949): 364–365.

[38] Nicholas, Theodore. "Step loading for very high cycle fatigue." Fatigue & Fracture of Engineering Materials & Structures 25.8-9 (2002): 861–869.

[39] Koutiri, Imade, et al. "High cycle fatigue damage mechanisms in cast aluminium subject to complex loads." International Journal of Fatigue 47 (2013): 44–57.

[40] Brugger, C., et al. "Ultrasonic fatigue testing device under biaxial bending." Frattura ed Integria Strutturale 37 (2016): 46–51.

[41] Kamaya, Masayuki. "Development of disc bending fatigue test technique for equi-biaxial loading." International Journal of Fatigue 82 (2016): 561–571.

[42] Gourdin, C., et al. "Equi-biaxial loading effect on austenitic stainless steel fatigue life." Frattura ed Integrità Strutturale 38 (2016): 162.

[43] Vingsbo, Olof, and Staffan Söderberg. "On fretting maps." Wear 126.2 (1988): 131–147.

[44] Weibull, Waloddi. "Fatigue testing and analysis of results." Elsevier (2013).

[45] Zouani, A., T. Bui-Quoc, and M. Bernard. "Optimal design of a disk-shaped specimen for biaxial-tensile fatigue testing." Journal of testing and evaluation 24.5 (1996): 287–294.

[46] Ferron, G., and A. Makinde. "Design and development of a biaxial strength testing device." Journal of Testing and Evaluation 16.3 (1988): 253–256.

[47] Lempert, G. D., and A. Tsour. "Reduction of static friction between surfaces of Ti-6Al-4V and between surfaces of Ti-6Al-4V and Al-7075." Surface and

Coatings Technology 52.3 (1992): 291–295.

[48] Bhandari, V. B. "Machine Design Data book." McGraw-Hill Education (2014).

A

Comparison of Criteria – Varying Amplitude Stress

The criteria predictions for various states of amplitude stress is investigated. It is assumed that no mid stresses are present. Predictions from Sines and Findley criteria vary only slightly. With no mid stresses, Manson–McKnight and Sines yield the same results.

Dang Van and Crossland deviate from the others. Here a larger influence of amplitude stress state can be observed. For a biaxial amplitude stress, i.e. $\sigma_{1,a} = \sigma_{2,a}$, these two criteria are more conservative. This explains why these curves are far below the others in Figure 4.2 and 4.4.

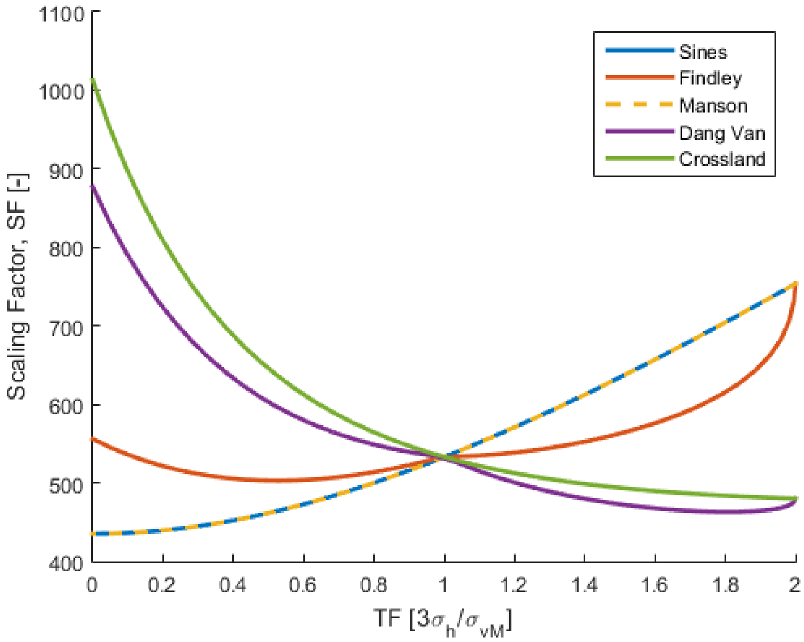

Figure A.1: Influence of varying amplitude stress states.

B

Biaxial Stress from Uniaxial Load

To be able to use conventional uniaxial testing machines, different concepts have been suggested. Two interesting and innovative concepts can be seen in Figure B.1a and B.1b. These are used in [45] and [46] respectively.

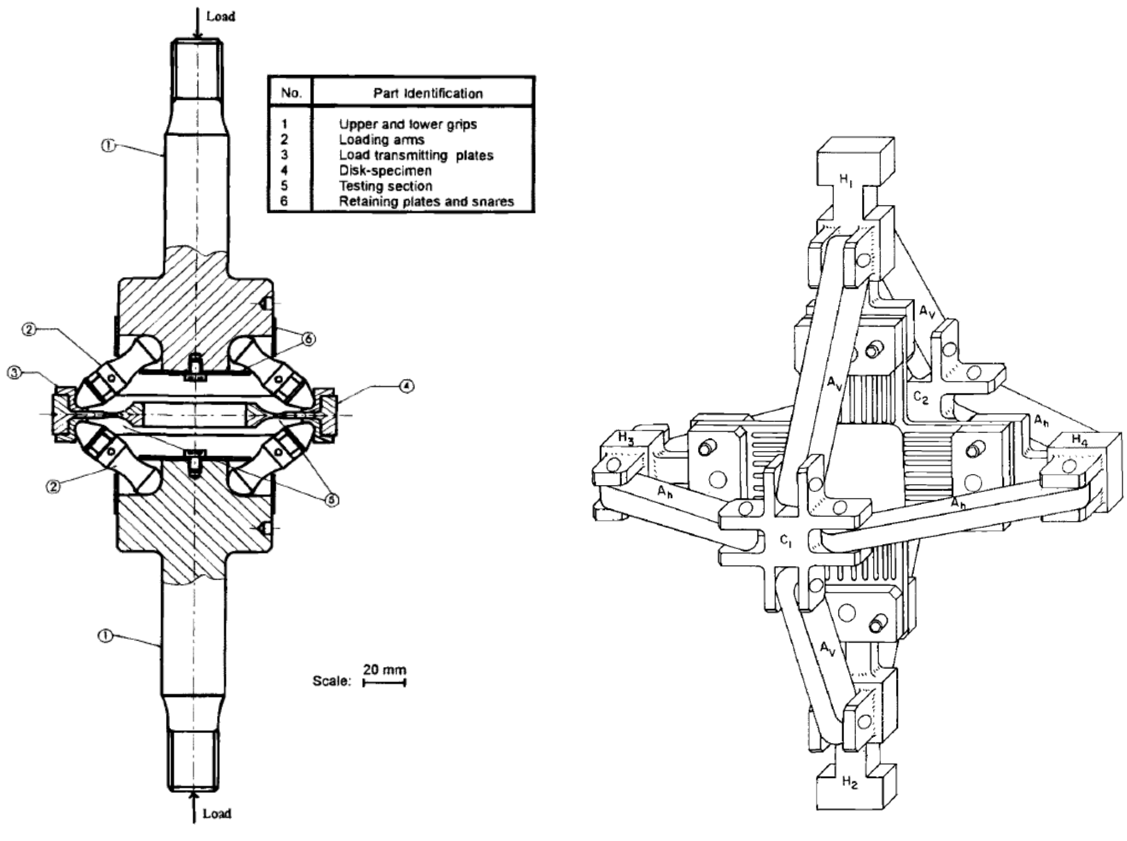

(a) **(b)**

Figure B.1: Biaxial testing techniques using uniaxial loading, (a) from [45] and (b) from [46].

C

Vibrating Disc – Various Geometries

Some results from the development of the vibrating disc concept are presented in this Appendix.

C.1 Pre-bending of Disc

The idea of pre-bending showed some shortcomings. The stress stiffening effect of the disc (captured with large deformation analysis in the FE-simulations) caused stress concentrations close to the fixture, as can be seen in Figure C.1. For testing purposes, the fatigue region should be positioned in the middle of the plate and corresponding to a more homogeneous stress field. Therefore, pre-bending as a way of producing the mid stress was rejected.

Figure C.1: Stress distribution from pre-bending.

C.2 Disc with Constant Thickness

A disc with constant thickness was evaluated. The pre-stress was generated as in-plane tension. The mid stress will be uniform through the disc, as can be seen in the lower half of Figure C.2. The amplitude stress from the vibrational motion are shown in the upper half of Figure C.2. Stress concentrations occur close to the edge. With the same argument as for pre-bending, this will be an unsuitable stress field for testing purposes.

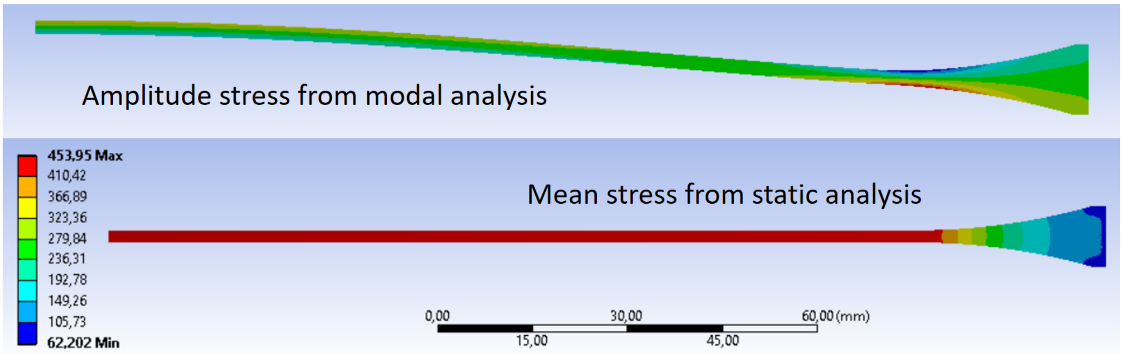

Figure C.2: Stress distribution in disc with constant thickness.

It is worthwhile noting that the stress concentration near the edge is caused by the prestress. If the disc was unloaded when set into first vibration mode, the stress would reach its maximum magnitude in the middle of the disc. This is displayed in Figure C.3.

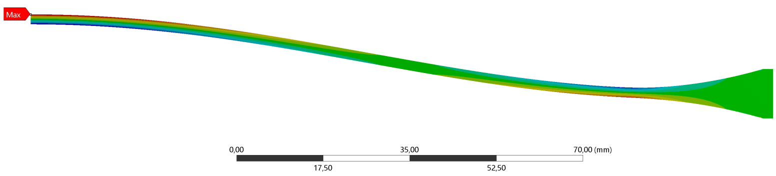

Figure C.3: Stress distribution from vibrational mode in a disc without prestress.

C.3 Disc with Centre Thickness Reduction

In order to concentrate stresses in the middle region of the disc, a thickness reduction is introduced. The nominal thickness is 4 mm, whereas the center thickness is 2 mm. As can be seen in the upper half of Figure C.4, the amplitude stress reaches maximum on the upper surface in the middle region. From this point of view, this concept performs better than the constant thickness displayed in Figure C.2. The mid stress, seen in lower half of Figure C.4, also reaches maximum values in the middle but on the lower surface. There will be quite a steep gradient through the thickness. Once again, maximum levels of mid and amplitude stresses do not occur in the same region.

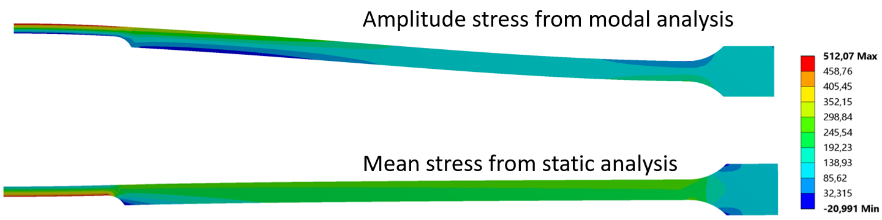

Figure C.4: Stress distribution in disc with centre thickness reduction.

D

Shrink Fit – Additional Theory and Results

D.1 Basic Equations

The stress state for a cylinder with internal pressure can be obtained analytically. The variation through the thickness for the radial stress, σ_r, and the hoop stress, σ_ϕ are given by the following equations:

$$\sigma_r = \frac{r_1^2(r^2 - r_2^2)}{r^2(r_2^2 - r_1^2)}p \tag{D.1}$$

$$\sigma_\phi = \frac{r_1^2(r^2 + r_2^2)}{r^2(r_2^2 - r_1^2)}p \tag{D.2}$$

Where p is internal pressure, r_1 is the inner radius and r_2 is the outer radius, see Figure D.1. This means that the radial stress will vary from $-p_i$ at the inner surface to zero at the outer surface. The hoop stress will also be greatest at the inner surface and decreasing towards the outer surface, see illustration in Figure D.1.

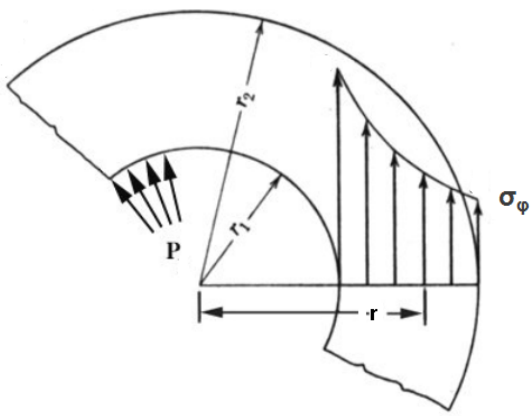

Figure D.1: Cylinder dimensions and distribution of hoop stress through thickness.

If the thickness is smaller than one-tenth of the radius, the equations of thin-walled cylinders are a good approximation:

$$\sigma_r \approx 0 \ll \sigma_\phi \tag{D.3}$$
$$\sigma_\phi = \frac{pr}{2t} \tag{D.4}$$

This means that the radial stress is very small compared to the hoop stress and that the hoop stress is close to constant through the cross section. Since a uniform stress distribution is desired in the tubular specimen, the test section should be thin-walled.

The internal pressure from the shrink fit is dependent on the interference, according to:

$$p = E\delta_r \frac{r_2^2 - r_1^2}{2r_1 r_2^2} \tag{D.5}$$

Where the radial interference, δ_r, if obtained from thermal expansion/contraction, can be calculated as:

$$\delta_r = \alpha \Delta T r_1 \tag{D.6}$$

Where α is the thermal expansion coefficient and ΔT is the temperature difference. The demands are set on the maximum hoop and axial stress that should be reached:

$$\sigma_a = 800MPa \tag{D.7}$$
$$\sigma_\phi = 400MPa \tag{D.8}$$

D.2 Assumptions made in the simulations

First of all, an estimate of the shrink fit interference must be made. The material to be tested, Ti-6Al-4V (material data taken from [17]), is possible to heat around 450°C, staying below the phase transformation temperature approximately 500°C. Furthermore, the solid shaft, made in the same material, may be cooled in liquid nitrogen to around −190°C. This gives a potential ΔT of 640°C, corresponding to a diametrical interference of 144 microns for a 25 mm hole.

The tolerances must be tight to obtain the desired shrink fit interference. An IT-grade of IT5 should be possible for the manufacturing of the hole, where precision boring, fine internal grinding and honing is required according to [48]. The same grade should also be possible for the shaft, meaning tolerances around ±5 microns each. From the possible temperatures and tolerances stated above, the diametrical interference is estimated in the range from 90 to 110 microns. In the simulations presented below, 90 microns is used.

Furthermore, to assess the risk of slippage, the friction must be estimated. Experimental values of static friction between surfaces of Ti-6Al-4V is reported as $\mu = 0.38 \pm 0.02$ in [47]. Therefore, a value of 0.36 is used. The contact modelling in the FE-model is made through non-linear analysis using the Augmented Lagrange Method. This turned out to be mesh sensitive, requiring a fine mesh in the contact region for converging results.

D.3 Initial Geometry

As a starting point, a geometry for typical tubular specimen were used, as shown in Figure 6.21 (found in [3]). For this geometry, the effective stress distribution is shown in Figure D.2. The critical point is located in the interface where the hoop stress reaches its maximum value, as illustrated in Figure D.1. Only small axial forces can be applied before slip occurs, so that the desired stress levels are not reached. Through a manual process, a better geometry is developed. These results are presented in Section 6.4.

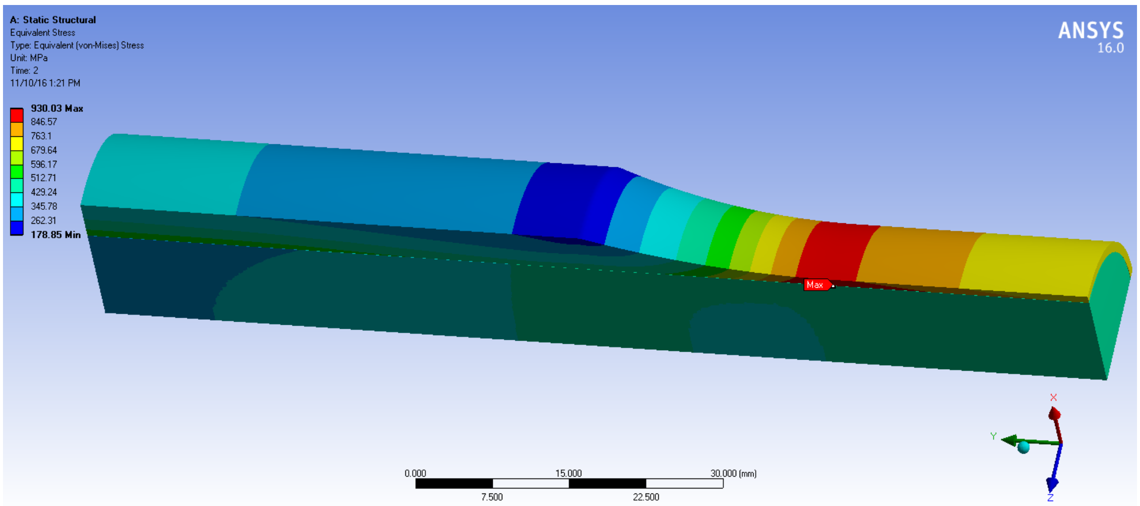

Figure D.2: Von Mises effective stress distribution for initial geometry.